Bioengineered GelMA Tooth Bud Constructs for Future Applications in Regenerative Dentistry

A thesis submitted by

Elizabeth Smith

in partial fulfillment of the requirements for the degree of

PhD

in

Cell, Molecular, and Developmental Biology

Tufts University

Sackler School of Graduate Biomedical Sciences

May 2018

Adviser: Pamela Yelick, PhD

Abstract

Tooth loss is a prevalent disease that affects millions of people worldwide. Loss of natural teeth can contribute to physiological and social disadvantages while reducing the quality of life. The exciting emerging field of Regenerative Dental Research aims to use biologically-based tissue engineering techniques to create bioengineered dental tissue and whole tooth replacement therapies. This innovative approach will provide function and responsiveness similar to natural teeth and serve as an alternative to currently used artificial materials.

The basic goal of tissue engineering is to repair or replace damaged or lost tissues by utilizing a combination of cells and supportive scaffolds. The work described here is focused on the characterization and optimization of a three-dimensional (3D) tooth bud model composed of postnatal dental progenitor stem cells and HUVECs encapsulated within Gelatin Methacryloyl (GelMA) hydrogel scaffold. Preliminary *in vitro* results showed that GelMA hydrogels can be tuned to resemble mechanical characteristics of the natural tooth bud microenvironment. Also, encapsulated dental cells and HUVECs exhibited increased attachment, metabolic and MMP activities overtime. Furthermore, *in vitro* capillary-like networks formed within the 3D tooth bud model. *In vivo* implanted tooth bud constructs demonstrated functional vascular networks that circulated host red blood cells (RBCs) and mineralized tissue that adopted the size and shape of the original construct.

Optimization of the GelMA tooth bud model aimed to assess the effect of various cell seeding densities and fabrication techniques. Optimized tooth bud constructs showed

evidence of many features of natural tooth buds. This includes a putative dental epithelial stem cell (DESC) niche, a basement membrane, Wnt signaling, bioengineered enamel knot (EK) signaling center, transit amplifying (TA) cells, and fibrillin expression that resembled that of early tooth development. These results are the first to report the recapitulation of the natural DESC niche and other features of natural tooth development using postnatal dental cells.

All of the results presented here, suggest that GelMA hydrogel is a promising scaffold material that can be used in future applications for bioengineering dental tissues and excitingly, whole teeth replacements in humans. Future studies focus on advancing this 3D tooth bud model towards clinical applications.

Dedication

This work is dedicated to my personal support system of family and friends: my fiancée, Eddie Frierson, who put his life on hold to fully support my efforts and ensure my sanity; my Mom and Dad, Beverly and Clarence Smith who never doubted my abilities to pursue my dreams; my sister, Christina Harris, who encouraged me throughout the toughest times and was always there to boost my confidence; and my comrade, Melissa Liriano who I admire for her brilliance, confidence, and her unending ability to offer her ear whenever requested.

Acknowledgements

I would like to acknowledge the following people: my thesis advisor and mentor, Dr. Pamela C Yelick, who taught by example that there is no obstacle too high to overcome; members of my thesis advisory committee Dr. Li Zeng, Dr. Heber Nielsen, and Dr. Lauren Black III, who encouraged all of my ambitious efforts; Dr. Weibo Zhang, who made herself limitlessly available for advice, suggestions, and hands-on training. I would also like to thank past and present members of the Khademhosseini Lab that provided the GelMA material and endless advice and support; Dr. Nelson Monteiro who was a wonderful source for general advice, especially regarding work-life balance; Shantel Angstadt, a former technician whose work ethic and enthusiasm was refreshing (best of luck at John Hopkins!); Dr. Rachel Skvirsky, Dr. Adán Colón-Carmona, Dr. Juan Carlos Vega-Hernandez, Dr, Alexei Degterev, Dr Henry Wortis and those involved with Tufts PREP program who all helped me to realize my full potential to pursue a PhD degree in the biomedical science field. I would also like to thank my thesis program and the supportive staff along with the Sackler School of Graduate Biomedical Sciences at Tufts University. Lastly, I would like to acknowledge the funding that supported this project, granted by NIH/NIDCR.

Table of Contents

List of Tables

List of Figures

List of Copyrighted Materials Produced by the Author

1. Smith EE, Yelick PC (2016) Progress in bioengineered whole tooth research: from bench to dental patient chair. Current Oral Health Reports. 3(4): 302-308. DOI: 10.1007/s40496-016-0110-2.

2. Smith EE, Zhang W, Schiele NR, Kuo CK, Khademhosseini A, Yelick PC (2017) Developing a biomimetic tooth bud model. Journal of Tissue Engineering and Regenerative Medicine. DOI: 10.1002/term.2246.

List of Abbreviations

1D-7D – 1 Day (in normal growth media) – 7 Days (in osteogenic media)
3D - Three dimensional
7D-7D – 7 Day (in normal growth media) – 7 Days (in osteogenic media)
Arg-Gly-Asp – Arginine-Glycine-Aspartate
AM – Amelogenin
B-Cat – Beta-Catenin
BMP – Bone Morphogenetic Protein
CD31 – Cluster of Differentiation 31
DE – Dental Epithelium/epithelial
DESC – Dental Epithelial Stem Cell
DFPC – Dental Follicle Precursor Cells
DPSCs – Dental Pulp Stem Cells
DSC – Dental Stem Cells
DSPP – Dentin Sialophosphoprotein
DM – Dental Mesenchyme/mesenchymal
ECAD – E-CCadherin
ECM – Extracellular Matrix
EK – Enamel Knot
ERM – Epithelial Cell Rests of Malassez
Fib1 – Fibrillin-1
Fib2 – Fibrillin-2
FGF – Fibroblastic Growth Factor
FV-AFM – Force Volume-Atomic Force Microscopy
GelMA – Gelatin Methacrylate/Methacryloyl
H&E – Hematoxylin and Eosin
HUVECs – Human Umbilical Vein Endothelial Cells
IF – Immunofluorescent
IHC – Immunohistochemistry
iPSc – Induced Pluripotent stem cells
Lef-1 – Lymphoid Enhancer Binder Factor 1
MSCs – Mesenchymal Stem Cells
MMP – Matrix Metalloproteinase
OC – Osteocalcin
pDE – Postnatal porcine Dental Epithelium/epithelial
PDLSCs – Periodontal Ligament Stem Cells
pDM – Postnatal porcine Dental Mesenchyme/mesenchymal
PI – Photo Initiator
PLLA – Poly-L-Lactic Acid
PLGA – Poly-Lactic-co-Glycolic Acid
RBCs – Red Blood Cells
SCAP – Stem Cells of the Apical Papilla

SHED – Stem Cells of Human Exfoliated Deciduous Teeth
SHH – Sonic Hedgehog
Sox-2 – Sex Determining Region Y – Box 2
TA – Transit Amplifying
TGFβ1 – Transforming Growth Factor Beta 1
VM – Vimentin

Chapter 1: Introduction

1.1 Bioengineering Whole Teeth

As a highly prevalent disease, tooth loss affects over 158 million people worldwide (*1*). Craniofacial birth defects, poor dental hygiene, battlefield injuries, accidental and intentional traumatic injuries all can contribute to tooth loss. Currently, artificial dental implants are the most commonly used tooth replacement therapy. Unfortunately, dental implants are prone to failures, and are associated with complications such as tissue and bone loss around the implant site, fracture, peri-implantitis, infections and inflammation. (*2, 3*). All of these issues highlight the clinical need for dental implant alternatives, including biologically based replacement teeth as superior alternatives to artificial dental implants (*4, 5*).

Ideally, bioengineered teeth would be generated using autologous dental cells extracted from an individual patient, such as those harvested from an extracted wisdom tooth, which would then be expanded in in vitro tissue culture. Once sufficient numbers of cells are generated, they would then be incorporated within a scaffold, and implanted at the site of tooth loss, where it would be expected to develop, erupt and function like a natural tooth. This regenerative therapy approach will only become a reality in the clinic once extensive investigation identifies postnatal dental cells sources, appropriate scaffold materials and fabrication, and inductive factors that can be readily used for devising bioengineered teeth that resemble natural teeth (Figure 1.1).

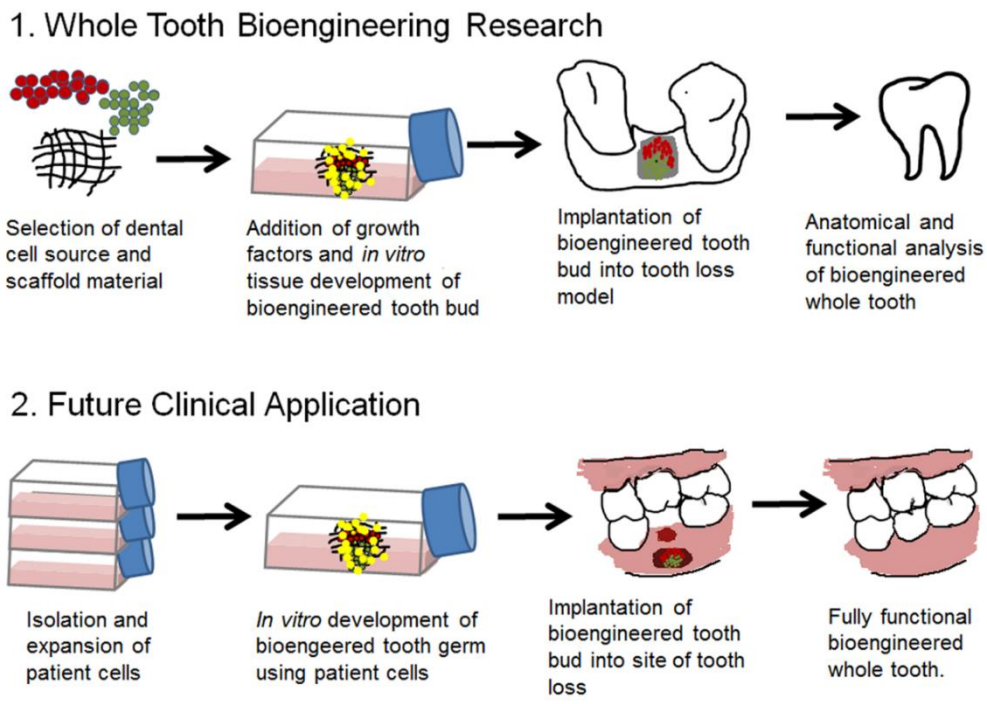

Figure 1.1 Models for Whole Tooth Bioengineering. (1) Research objective. In order for whole tooth bioengineering to become a reality in a clinical setting, extensive research must be conducted. This research includes identifying suitable cell sources and scaffold materials that support the in vitro development of a bioengineered tooth bud for implantation into a tooth loss model. (2) Future clinical applications. Once appropriate materials have been validated, they should be easily translatable for clinical application of using patients own cells to correct an area of tooth loss by regenerating a fully functional tooth.

Natural teeth are highly complex organs composed of hard mineralized tissues, including enamel, dentin, and cementum, and soft tissues including dental pulp and periodontal ligament (*6*). All of these tissues originate from the ectoderm-derived dental epithelium and the neural crests derived dental mesenchyme, whose early interactions initiate and subsequently support reciprocal and reiterative signaling throughout tooth development (*7*, *8*). The initiation of tooth development is defined by a thickening of the oral epithelium that then invaginates into the underlying dental mesenchyme. The surrounding dental mesenchyme then condenses, leading to morphogenesis of the dental

epithelium and dental cell differentiation (*6, 9, 10*). Dental epithelial-derived ameloblasts are the differentiated cells that are responsible for enamel production, while differentiated dental mesenchymal-derived odontoblasts produce dentin (*5, 8, 11, 12*). The process of tooth development is regulated by the interactions of the dental tissues – dental epithelium and dental mesenchyme. It has been shown that if this interaction is prevented, tooth development will not progress (*13-15*). It has also been demonstrated by classical tissue recombinant studies that the odontogenetic potential, or the instructional capability of the dental tissues and cells, is conserved even after tissue dissociation and in vitro culture (*16*). These concepts that drive natural tooth development provide an instructive guide for optimal conditions that can be used to create bioengineered whole teeth.

1.2 Dental Cell Sources for Whole Tooth Bioengineering

Embryonic dental stem cells, harvested from mice and/or rats, have commonly been used in many historic and current tooth regeneration studies due to their significant odontogenic potential. However, human embryonic cells cannot be used as a clinically relevant human dental cell source due to unavoidable ethical issues, potential for immune reaction and rejection, and malignant potential. Current embryonic dental stem cell alternatives focus on using postnatal dental stem and progenitor cells isolated from adult dental epithelial and dental mesenchymal tissues. Prior published reports have demonstrated the odontogenic potential of postnatal (adult) dental epithelial and dental

mesenchymal single cell suspensions, including the ability to produce anatomically accurate tooth crowns consisting of dentin, pulp, and enamel. (*17-19*).

Today, the most common source of dental mesenchymal stem cells being used for tooth regeneration research is postnatal dental pulp stem cells (DPSCs). The dental pulp contains an enriched population of stem cells that can be easily isolated. In numerous studies, DPSC have been shown to differentiate into odontoblasts and osteoblasts, and to form pulp, dentin, and cementum tissues respectively (*20-23*). Stem cells of human exfoliated deciduous teeth (SHED) can be isolated from the pulp of primary human teeth, and have demonstrated capacity to differentiate into odontoblasts, and to produce dentin-like and pulp-like tissues (*24, 25*). SHED can be extracted from a very accessible source – human baby teeth - and have the ability to provide an adequate number of cells for regenerative dental applications (*24*). Stem cells of the apical pallia (SCAP) are isolated from pulp tissue located within open roots of developing baby teeth (*26*), and have been shown to differentiate into odontoblasts and osteoblasts, and to form dentin-like structures. (*27*). Dental follicle precursor cells (DFPCs) are mesenchymal cells that surround and enclose the developing tooth bud, and which will eventually contribute to the periodontal ligament and cementum tissues (*28*). DFPCs are able to differentiate into cementoblasts that form cementum, and to periodontal ligament-like tissues (*28*), and have been found to be suitable for dentin regeneration (*29*). Similarly, Periodontal Ligament Stem Cells (PDLSCs) have been shown to differentiate into cementum-forming cementoblasts, as well as periodontal ligament-like tissues (*30*). In addition, when

PDLSCs were combined with DPSCs, root-like and dentin-like structures were formed (*20*).

Various tissue sources have also been investigated to successfully generate dental epithelial cells that can differentiate into enamel-secreting ameloblasts. For example, dental epithelial cell rests of Malassez (ERM) have the ability to differentiate into ameloblast like cells and to produce enamel when combined with dental pulp cells (*31*). Another study showed that when cells from the enamel organ were combined with dental mesenchymal cells, enamel-dentin structures were formed (*32*). It has also been shown that skin epithelial cells have the ability to express ameloblasts markers when cultured with dental pulp cells (*33*). Finally, adult human gingival cells have the ability to form enamel structures when combined with dental mesenchymal cells (*34*). Any or all of these dental epithelial cell sources may prove promising for effective whole tooth tissue engineering applications.

Recently, investigations using induced pluripotent stem cells (iPSCs) for tooth regeneration research have increased. These cells are pluripotent and therefore have the ability to develop into a variety of cells types (*35-37*). It has been shown that gingival cells, SHED, SCAP, DSCPs, and periodontal ligament cells can all be used to create iPSCs (*38-40*). In addition, iPSCs have been shown to exhibit the ability to differentiate into ameloblast-like and odontoblast-like cells (*41, 42*).

The field of tooth tissue engineering and regenerative dentistry has investigated this wide variety of cell types to identify sources that can easily be accessed and utilized for clinical dental applications. The knowledge gained from the use of the cells

mentioned above has helped to further our understanding and appreciation of how they can be combined and utilized to advance whole tooth bioengineering research. Also, it was recently reported that a scaffold-free method can be used to examine the usefulness of various cell sources for the use in tooth regenerative studies (*43*). In addition, a recent study has demonstrated that recombination of postnatal dental epithelial and dental mesenchymal tissues have the ability to form tooth structures, offering an alternative to single cell suspension techniques in whole tooth regeneration (*44*).

1.3 Scaffold Materials and Bioprinting for Tooth Tissue Engineering

Appropriate selection of scaffold materials is very important for regenerative dental applications, as the microenvironment provides cellular support and mechanical cues that affect cell behavior. For example, it has been shown that hydrogel scaffold stiffness can influence the fate of mesenchymal stem cells (*45*). In addition, scaffold materials must allow cellular attachment, spreading, proliferation, and differentiation to allow the development of the desired tissues. Furthermore and ideally, scaffold degradation rate should match the rate of extracellular matrix (ECM) deposition by the cells, in order to ensure robust formation and durability of the bioengineered tissue (*46*). An extensive variety of natural and synthetic scaffold materials have been investigated for tooth regeneration applications (*46-48*). One group of materials that has been examined are poly-L-lactic acid (PLLA)/ polylactic-co-glycolic acid (PLGA) polymers (*49-51*). PLLA, PLGA and their derivatives are synthetic polymers that can be readily prepared. Hydrogel-based materials such as collagen, gelatin, and alginate are highly

tunable, and have been used to successfully bioengineer various dental tissues (*21, 22, 32, 52*). Silk-based materials have also shown promise in providing an environment that can support osteo-dentin-like mineralized tissue formation, but further optimizations are needed to enhance bioengineered dental tissue formation (*53, 54*). A combination of these and other novel materials may eventually be used to successfully engineer the wide variety of hard and soft tissues that comprise the natural tooth.

The size and shape of scaffold materials can be easily and meticulously generated with the use of 3D printing (*55*). This fabrication method deposits material layer by layer until a desired 3D structure is produced (*56*). Today, 3D printers are able to dispense plastic, ceramics, biomaterials, and even cells in a highly organized manner (*56-58*). It has been suggested that 3D printing can be utilized in regenerative medicine to aide in the creation of complex bioengineered tissues and organs (*58, 59*). In addition, 3D printing can offer customizations on a patient to patient basis (*56, 60*).

1.4 Incorporation of Growth Factors

Growth factors are soluble proteins that direct the development of various tissues and organs. Several important growth factors are involved in natural tooth development, including bone morphogenetic protein (BMP), fibroblastic growth factor (FGF), and transforming growth factor beta 1 (TGFβ1) (*5, 8, 46, 61, 62*). The addition of these factors to bioengineered tooth constructs can therefore be used to enhance the successful generation of bioengineered whole teeth.

BMP4 is thought to play an important role in tooth morphogenesis by activating transcription factors in the dental mesenchyme (*63, 64*). BMP4, in combination with BMP2 and BMP7, regulate cell proliferation, tooth patterning and crown shape (*65-67*). Additionally, BMP4 is involved in ameloblast differentiation and tooth root formation (*68, 69*). Furthermore, it has been suggested that loss of bmp4 gene expression may account for the lack of teeth in birds (*70*). Roles for Bmp signaling in both dental mesenchymal and dental epithelial cell differentiation was further demonstrated by the differentiation of iPSCs into both odontoblastic and ameloblastic lineages, respectively, by the addition of exogenous BMP4. FGF signaling has been shown to be required for tooth morphogenesis (*71*). Decreased FGF signaling prevents tooth development (*71, 72*). TGFβ1 can induce odontoblast differentiation, pulp and dentin formation (*73-76*), and has been used to enhance the differentiation DPSCs into odontoblasts *in vitro* (*21*). These studies emphasize that selective incorporation of combinations of these growth factors into novel bioengineered tooth constructs could be used to enhance dental cell differentiation, and dental tissue and whole tooth formation.

1.5 Host Implant Models for Tooth Tissue Engineering

Small animals such as mice, rats, ferrets and rabbits are ideal for *in vivo* tooth regeneration studies that include a large number of samples, as their maintenance is more cost effective than large animals. Usual implantation sites in small animals, such as subcutaneous pockets and renal capsules, are selected based on their high vascular availability. Tooth extraction socket/implantation sites of smaller animals may be

difficult to perform and analyze because the operation area is small and delicate and their dentition is not similar to humans. Normally larger animals are used for more advanced studies of tooth construct jaw implants. Mini-pigs are commonly used for tooth/alveolar bone implantation studies because they have a dentition similar to humans (*77, 78*). It has been suggested that the implantation site is important as it may influence the morphology of the bioengineered tooth (*21*). Therefore, knowing how, when, and where to place the bioengineered tooth implant can greatly affect its outcome.

1.6 Current Progress and Challenges in Whole Tooth Regeneration

The ideal bioengineered whole tooth would mimic the development, function and appearance of a natural tooth. To date, only a handful of studies have demonstrated the successful generation of fully functional bioengineered teeth, by implanting bioengineered tooth constructs composed of embryonic dental cells that were implanted and grown in mice tooth extraction sites (*79-81*). As already mentioned, the clinical relevance of these studies is hindered by the fact that embryonic stem cells, versus adult stem cells were used. Nevertheless, these studies can be used to guide strategies to generate bioengineered whole teeth for the use of human tooth replacement. One of the earliest successful whole tooth regeneration studies used single cell suspensions of postnatal dental cells to engineer whole tooth crowns consisting of dental pulp, dentin, enamel, and tooth root tissues (*49*). These anatomically correct tooth crowns were imperfect, in that they were very small and did not conform to the size and shape of the scaffold. Since then, additional studies have focused on identifying appropriate sources of

adult dental cells, optimal scaffold materials, and growth factor combinations that can properly direct the regeneration of functional bioengineered tooth. A recent report describes the use of a gelatin-chondroitin-hyaluronan scaffold seeded with postnatal dental cells implanted into a healed mandibular tooth extraction site of an adult Lanyu miniature pig, to successfully generate enamel-like tissues, dentin, cementum, and developing tooth roots (*21*). Further improvements to this model, including validation that the purported bioengineered tooth was in fact not a natural pig replacement tooth, as well as functional analysis of these bioengineered teeth, would significantly improve the significance of this study.

Today, the major challenges facing the field of whole tooth bioengineering are identifying reliable sources of dental epithelial cells for clinical applications, and optimizing methods to fabricate scaffolds that can promote and accommodate the organized growth of all of the various hard and soft dental tissues, to form functional bioengineered teeth of specified size and shape. Additionally, bioengineered teeth must be sufficiently vascularized and integrated within the recipient anatomy. Overcoming these challenges may eventually contribute to emerging alternatives such as in bio-hybrid teeth, composed of both bioengineered living tissue and artificial materials (*20, 82*).

1.7 Conclusions and the Future of Whole Tooth Tissue Engineering

Whole tooth bioengineering is an exciting field that has emerged to provide an alternative to dental prosthesis currently used to treat the large numbers of people suffering from tooth loss. Although dental prosthetics historically have been the hallmark

of tooth replacement therapy, associated complications reveal the need for significant improvements. The field of whole tooth bioengineering research has demonstrated distinct accomplishments during its relatively short life. However, current research efforts must be directed to focus on the challenges and limitations that currently block our ability to reliably create clinically relevant bioengineered replacement teeth. Still, recent accomplishments indicate that despite the fact that teeth are complex organs composed of a wide variety of soft and hard tissues, whole tooth bioengineering for human tooth replacement is indeed possible, and in fact is the future of dentistry.

The written work presented here, describes the validation, characterization, and optimization of a tooth bud model intended as a future platform for whole tooth regeneration in human dentistry. The tooth bud model is composed of post-natal porcine dental epithelial and dental mesenchymal cells along with HUVECs embedded within a hydrogel material, Gelatin Methacryloyl (GelMA). We hypothesized that GelMA hydrogels can be used as a supportive scaffold for the formation of 3D biomimetic tooth buds of predetermined size and shape.

Preliminary studies aimed to validate GelMA as an appropriate hydrogel scaffold for the differentiation of encapsulated dental cells. These early studies also showed that GelMA can be tuned to resemble the natural tooth bud microenvironment. Additionally, after subcutaneous implantation, the formation of mineralized tissue adopted the size and shape of the GelMA scaffold.

More recent studies focused on optimizing the GelMA tooth bud model by varying a few of the initial parameters. Excitingly, this study resulted in the recapitulation

of several events that occur during natural tooth development, some which have never been reported using post-natal dental cells. All the of the results presented here support the GelMA tooth bud model as a promising step towards the future in regenerative dentistry.[1]

[1] This introduction is a modified version of Smith and Yelick 2016 (*125*), included with permission from Springer. To serve as a relevant introduction to the following work, changes include a summary of the hypothesis, results, and conclusions presented in the material that follows.

Chapter 2: Developing a Biomimetic Tooth Bud Model[2]

[2] Smith EE, Zhang W, Schiele NR, Kuo CK, Khademhosseini A, Yelick PC. *Journal of Tissue Engineering and Regenerative Medicine*. 10:1-11, 2017.
Reprinted here with permission of publisher.

2.1 Introduction

Mature teeth are highly complex mineralized organs that play vital roles in our everyday lives. It has been reported that over 158 million people globally are currently suffering from tooth loss (*83*). Synthetic dental implants are a common therapy for tooth loss. However, artificial implants may cause severe complications, such as peri-implantitis, bone loss, receding gums and periodontal tissues, and eventual implant failure (*2, 3*). Fully functional biologically based biomimetic teeth, that are vascularized and innervated, would be an attractive alternative to currently used artificial dental implants (*4, 5, 84*).

The present study describes the development and fabrication of a bioengineered, three-dimensional (3D) biologically based tooth bud model, designed to facilitate the dental epithelial (DE) and dental mesenchymal (DM) tissue interactions that occur in natural tooth development (*13*). Previously, it was shown that post-natal porcine and rat DE and DM cells, when seeded onto synthetic scaffolds, retained the ability to form small, anatomically correct tooth crowns consisting of enamel, dentin and pulp tissues (*17, 19, 49, 50*). These studies were the first to demonstrate the successful use of adult, post-natal (as opposed to embryonic) dental progenitor cells for whole tooth tissue engineering applications. However, an important limitation of these bioengineered teeth is that they were very small, and of unpredictable size and shape.

A novel biomimetic tooth bud model that employs post-natal dental cells encapsulated within tunable, photopolymerizable gelatin methacrylate (GelMA) hydrogel scaffolds is described. Dental cell-encapsulated GelMA constructs were designed to

facilitate organized DE-DE, DM-DM and DE-DM cell interactions leading to ameloblast and odontoblast differentiation, respectively, and the formation of bioengineered teeth of predictable size and shape. GelMA hydrogels are largely composed of denatured collagen, and retain many of collagen's natural properties including Arg-Gly-Asp (RGD) adhesive domains and matrix metallopeptidase (MMP) sensitive sites (*85*), which are known to enhance cell binding and cell-mediated matrix degradation, respectively. In addition, the physical properties of GelMA hydrogels can be tuned by varying GelMA and/or photoinitiator (PI) concentrations, to create scaffolds exhibiting elastic moduli approximating those of a variety of natural tissues. This versatile hydrogel has been used to successfully bioengineer contractile skeletal muscle, beating cardiac patches, functional vascular networks and endochondral bone (*86-90*).

To identify GelMA formulas suitable for bioengineered tooth development, individually encapsulated DE or DM cell GelMA constructs with elastic moduli similar to those of natural tooth bud derived enamel organ and pulp organ tissues. Human Umbilical Vein Endothelial Cells (HUVECs) were then included in these constructs to facilitate neovasculature formation within the constructs, and *in vivo* integration with host vasculature. The importance of the vasculature in the developing enamel organ and dental pulp has been well documented (*79, 91-93*); in addition, HUVECS have been demonstrated to promote neovascular formation in a variety of bioengineered tissues, and to facilitate *in vivo* engraftment with host vasculature (*94, 95*). Based on these studies, individual GelMA formula constructs were created that incorporated either porcine dental epithelial (pDE) cells and HUVECs (pDE-HUVECs) alone, or porcine dental

mesenchymal (pDM) cell and HUVECS (pDM-HUVECs) alone, respectively, and analyzed in 3D *in vitro* culture to monitor cell morphology, metabolic activity, and vascular network formation over time. Based on our promising *in vitro* results, constructs were then fabricated consisting of two different GelMA formulae: Gel 1 for encapsulated DE-HUVECs and Gel 3 for encapsulated DM-HUVECs. The resulting replicate 3D tooth bud constructs were created and cultured *in vitro* in osteogenic media, and subsequently either further studied *in vitro*, or implanted and grown subcutaneously in immunocompromised rats. Analyses of explanted *in vivo* tooth bud constructs revealed the formation of highly mineralized and vascularized bioengineered tooth constructs that approximated the size and shape of the original GelMA construct. This appears to be the first report to demonstrate the formation of vascularized biomineralized dental tissues from dental cell encapsulated GelMA constructs.

2.2 Materials and Methods

2.2.1 Primary dental cell isolation, *in vitro* culture and expansion

Three cell types were used to create bioengineered 3D GelMA tooth buds: (1) pDE cells, (2) pDM cells, and (3) HUVECs. Primary pDE and pDM progenitor cells were obtained and cultured as previously described (*18, 49*). Briefly, pDE and pDM progenitor cells were isolated from unerupted tooth buds extracted from 5-month-old porcine jaws. Single-cell suspensions were plated in DE or DM cell selective media and expanded in a humidified environment with 5% CO_2 at 37°C. HUVECs (PSC100010; ATCC, Manassas, VA, USA) were expanded in vascular basal media (PCS100030;

ATCC) with vascular endothelial growth factor (VEGF) growth kit (PCS10004; ATCC) in humidified 5% CO_2 at 37°C. All expanded cells were cryopreserved in 10% dimethylsufoxide (DMSO) in appropriate culture media until use.

2.2.2 GelMA cell encapsulation

Lyophilized GelMA was fully dissolved in DMEM/F12 media at the desired concentration, and photoinitiator (PI) (Irgacure2959; Sigma, St. Louis, MO, USA) was added to create three different GelMA formulas denoted Gel 1 (3% GelMA, 0.1% PI), Gel 2 (3% GelMA, 0.5% PI), and Gel 3 (5% GelMA, 0.1% PI) (Figure 2.1).

For *in vitro* analyses, acellular GelMA Gel 1-3 solutions, each containing either pDE-HUVECs or pDM-HUVECs, were each pipetted into replicate 6 mm diameter polydimethylsiloxane (PDMS) ring molds in 24-well plates. pDE-HUVECs (1:1) or pDM-HUVECs (1:1) (1.2×10^6 total cells per 20 µL) were suspended in GelMA Gel 1-3 solutions, and layered on top of a respective acellular GelMA layer. The resulting constructs were then photo-crosslinked by exposure to 9.16 W/cm2 UV light for 30 s an Omnicure S2000 (Lumen Dynamics Group Inc., Mississauga ON, Canada). After removal of the PDMS molds, the GelMA constructs were *in vitro*-cultured in osteogenic media [1:1:1 Dulbecco's Modified Eagle Medium (DMEM)/F12/LCH8/vascular basal media] supplemented with 1% Pen-Strep, 10% fetal bovine serum (FBS), 100 nM dexamethasone, 10mM beta glycerol phosphate, and 0.05 mM ascorbic acid for 1, 2, and 4 weeks.

Based on *in vitro* analyses, GelMA constructs were next created from selected Gel 1 and Gel 3 formulae as follows. pDM-HUVECs (1:1) were suspended in GelMA Gel 3 (0.6×10^6 cells per 20 µL) and pipetted into PDMS molds. Next, pDE-HUVECs (1:1) were suspended in GelMA Gel 1 (0.6×10^6 cells in 20 µL per sample) and layered on top of replicate pDM-HUVEC GelMA Gel 3 layers, followed by photo-crosslinking as described above. The resulting 3D tooth bud constructs were precultured *in vitro* in osteogenic media for 2 weeks. *In vitro*-cultured constructs were subsequently cultured for an additional 1 or 6 weeks *in vitro,* or implanted subcutaneously in nude rats for 1, 3 and 6 weeks.

2.2.3 Mechanical testing of natural dental tissues and GelMA constructs

Force volume-atomic force microscopy (FV-AFM) was used to measure the elastic modulus of natural porcine dental tissues compared with UV-crosslinked GelMA formula Gels 1, 2 and 3. Freshly harvested enamel organ and pulp tissues were biopunched to generate 6 mm diameter x 2 mm high tissue samples to size-match fabricated GelMA constructs. Cultured pDE and pDM cells were encapsulated in a 1:1 ratio (3.0×10^4 cells/µL) in each of the three GelMA formulae (Gel 1, Gel 2 and Gel 3). Acellular GelMA constructs were also included in these analyses. Whole-mount cell-encapsulated and acellular GelMA constructs were placed in Dulbecco's phosphate-buffered saline (DPBS) (#14190-250; Life Technologies, Carlsbad, CA, USA) and mechanically tested using a Dimension 3100 atomic force microscope (Bruker, Santa Barbara, CA, USA) as described previously (*96*). Indentation force curves were measured over 10×10 µm^2 areas at two separate locations using atomic force microscopy (AFM)

cantilevers with 0.06 N/m spring constants (Bruker) and 5 μm-radius SiO_2 spherical tips. The slopes of the linear region of the force-displacement curves were converted to elastic moduli using a spherical model of Hertzian indentation mechanics (*97*). All samples were measured in triplicate. Statistical analyses were performed as described below.

2.2.4 *In vivo* subcutaneous implantation

All animal surgeries were performed using approved Institutional Animal Care and Use Committee (IACUC) protocols and Mandatory Animal Care and Use (MACU) regulations. Replicate cell-encapsulated and acellular GelMA constructs were implanted subcutaneously onto the backs of immunocompromised 5-month-old female Rowett Nude rats (Charles River Laboratories, Willmington, MA, USA) and harvested after 1, 3, and 6 weeks of growth. Each rat host randomly received two cell-seeded and two acellular GelMA constructs. All samples were tested in at least six replicates.

2.2.5 Bioengineered GelMA tooth bud construct harvest and analyses

Harvested *in vitro* and *in vivo* constructs were fixed in 10% formalin overnight and washed in DPBS. Following X-ray analysis, mineralized constructs were immersed in fresh decalcification solution (22.5% formic acid +10% sodium citrate) every 3 days until fully decalcified. Decalcification was defined by lack of ammonium oxalate-calcium precipitate formation after 20 minutes. For paraffin sectioning, constructs were dehydrated through graded ethanol and xylenes, submerged in molten paraffin for 18 hrs, embedded in paraffin blocks and serially sectioned (6 μm thick) as described previously

(*98*). Hematoxylin and eosin (H&E) and PicroSirius Red (Polysciences, Warrington, PA, USA) stains were used to analyze selected sections.

For Immunofluorescent (IF) analysis, paraffin sections were blocked for 20 min in 5% bovine serum albumin (BSA) and incubated for 1 h with primary antibodies: mouse anti-Factor 8 (ab20721, 1:50; Abcam, Cambridge, MA, USA); and rabbit anti-Cytokeratin 14 (ab53115, 1:25; Abcam); or rabbit anti-vimentin (BS-0756R, 1:25; Bioss, Woburn, MA, USA). Sections were incubated an additional hour with fluorescent conjugated secondary antibodies anti-mouse IgG-Alexa Fluor 488 (515-545-003, 1:100; Jackson ImmunoResearch Laboratories, West Grove, PA, USA) and anti-rabbit IgG-Alexa Fluor 568 (A11011, 1:100, Invitrogen, Carlsbad, CA, USA). Sections were cover-slipped with 4',6-diamidino-2-phenylindole (DAPI) mounting medium (H-1500; Vector Laboratories, Burlingame, CA, USA).

For immunohistochemical (IHC) analyses, sections were incubated for 1 h with primary antibody: [mouse anti-hCD31 (ab187377, 1:20; Abcam; and LS-B5577, 1:20; LifeSpan BioSciencs, Seattle, WA, USA); rabbit anti-E-cadherin (ABIN1858334, 1:20; Antibodies Online, Atlanta, GA, USA); mouse anti-vimentin (sc-6260, 1:4000; Santa Cruz Biotechnology, Dallas, Texas, USA); mouse anti-osteocalcin (ab13418, 1:400; Abcam); rabbit anti-dentine sialophosphoprotein (GTX60194, 1:50; Genetex, Irvine, CA, USA); or rabbit anti-Amelogenin (ABT260,1:500-1:750, Millipore, Billerica, MA, USA). Sections were incubated for 45 min with Biotin-SP conjugated secondary antibody anti-mouse immunoglobulin G (IgG) (711-065-150, 1:500; Jackson ImmunoResearch) or anti-rabbit IgG (711-065-152, 1:500; Jackson ImmunoResearch), 45 min in ABC reagent

(PK-4000; Vector Laboratories), and 5 min in 3,3-diaminobenzidine (DAB) (D4293, Sigma, St. Louis, MO, USA, USA). All slides were counterstained with 0.1% fast green (F7252; Sigma).

2.2.6 MMP activities of cell-encapsulated GelMA tooth bud constructs

The activity of MMP was measured using a Sensolyte 390 Generic MMP Activity Kit (Anaspec, Fremont, CA, USA) following manufacturer's suggested protocol. Briefly, MMP substrate was added to each replicate sample (n=3) and incubated for 1 h at 37°C. Fluorescence was then measured using a MDC SpectraMax M5 Spectrophotometer (Molecular Devices, Sunnyvale, CA, USA).

2.2.7 Statistical analyses

GraphPad Prism5 Software (GraphPad Software, San Diego, CA, USA) was used to determine statistical significance via one-way ANOVA followed by the Sidaks multiple comparison test for the AFM results.

2.3 Results

2.3.1 Mechanical properties of GelMA constructs and natural dental tissue

GelMA formulas (Gels 1, 2 and 3) were created by varying the GelMA and/or photoinitiator (PI) concentrations as indicated in (Figure 2.1). The elastic moduli of GelMA formulas Gels 1, 2 and 3, and of natural porcine dental pulp and enamel organ tissue samples were measured using FV-AFM (Figure 2. 1). The results showed that acellular GelMA Gel 1 exhibited the lowest elastic modulus (2.33 ± 0.19 kPA), while

acellular GelMA Gel 2 and Gel 3 exhibited elastic moduli of 4.19 ± 0.55 kPA and 4.47 ± 0.74 kPA, respectively (Figure 2.1). The AFM results also demonstrated that pDM cell seeded GelMA Gel 3 constructs exhibited elastic moduli similar to that of natural dental pulp tissue, 2.45 ± 0.03 kPA and 2.39 ± 0.26 kPA, respectively (Figure 2.1). The elastic moduli of dental cell-encapsulated GelMA Gels 1 and 2, and of pDE enamel organ tissue, were all below the limits of detection using this approach (Figure 2.1). Together, these results indicated that the elastic moduli of selected GelMA formulas were within a range similar to those of natural dental tissues.

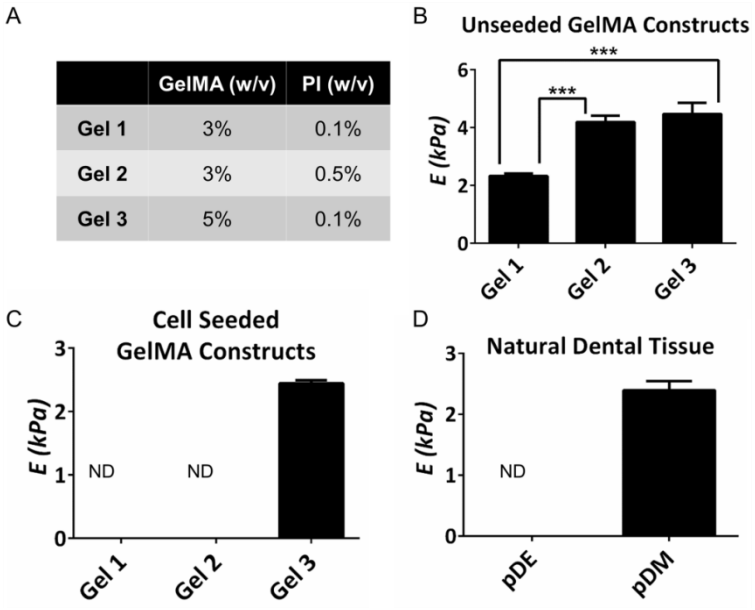

Figure 2.1: Comparative elastic moduli of gelatin methacrylate (GelMA) constructs and natural porcine dental tissues. (a) GelMA Gel formulae with corresponding GelMA and photoinitiator concentrations (% *w/v*). Elastic moduli of (b) unseeded GelMA constructs, (c) porcine dental epithelial (pDE)–porcine dental mesenchymal (pDM) cell-encapsulated GelMA constructs, and (d) natural porcine dental tissues. Dental cell-seeded Gel 3 had similar elastic modulus to that of pDM tissue. Bar graphs represent average ± SD (n = 3). ND, not determined (elastic modulus below detection level). ***$p \leq 0.001$; ANOVA followed by Sidak's comparison.

2.3.2 *In vitro* characterization of bioengineered GelMA constructs

2.3.2.1 Gross and cellular morphologies of 3D bioengineered GelMA constructs

Bright field microscopy was used to monitor the gross morphology of individual pDE-HUVEC-encapsulated, or pDM-HUVEC-encapsulated GelMA constructs over 4 weeks of *in vitro* culture. As previously reported, it was observed that dental cell encapsulated Gel 1 and Gel 3 GelMA constructs shrunk in size over time in culture (*99*), likely the result of encapsulated cell attachment and force exerted on the surrounding hydrogel (*100-103*). Shrinkage of pDE-HUVEC-encapsulated constructs appeared somewhat greater in Gel 1 as compared to Gels 2 and 3, while pDM-HUVEC encapsulated constructs exhibited greatest contraction in Gel 3 (*99*). All acellular GelMA constructs, and cell seeded Gel 2 constructs, retained their size and shape over time in culture (*99*).

In addition, distinct morphological changes were observed in GelMA Gel 1 and Gel 3 encapsulated cells, including cell spreading and clustering (Figure 2.2, arrowheads). In contrast, GelMA Gel 2 encapsulated cells remained as individual, round cells over time in culture (Figure 2.2, arrows). These results signify that pDE-HUVECs and pDM-HUVECs encapsulated in GelMA Gels 1 and 3 exhibited cell attachment and spreading, while those in Gel 2 did not.

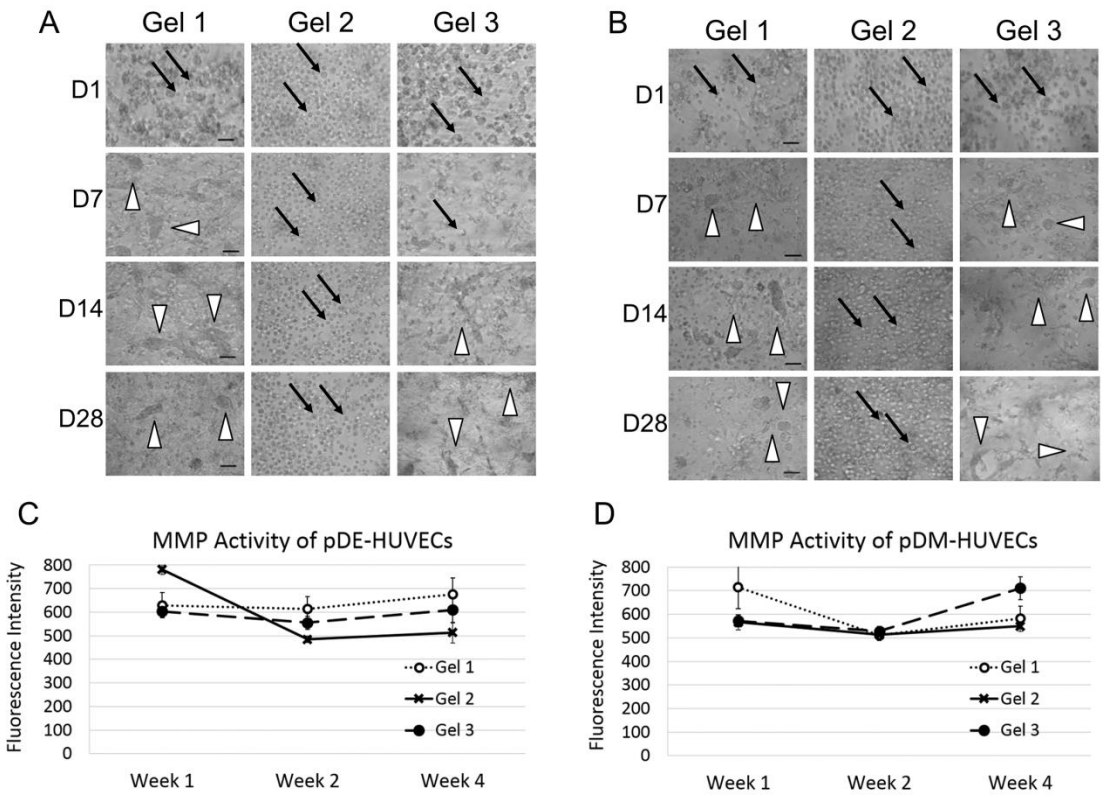

Figure 2.2. Morphology and MMP activity of *in vitro* cultured GelMA encapsulated cells. Bright field images of (A) pDE-HUVEC and (B) pDM-HUVEC GelMA Gel 1, Gel 2 and Gel 3 constructs over 28 days in culture. (C, D) MMP activities of *in vitro* cultured (C) pDE-HUVECs and (D) pDM-HUVECs GelMA constructs. pDE-HUVEC and pDM-HUVECs exhibited increased cell spreading and organized cell network formation (A, B arrowheads) in Gel 1 and Gel 3 over time in culture as compared to Gel 2 (A, B arrows). Quantified MMP activity of encapsulated pDE-HUVEc slightly increased in GelMA Gel 1 and Gel 3 over time in culture (C). pDM-HUVECs exhibited increased MMP activity in GelMA Gel 3 constructs (D). Data points are averages ± SE. (n=6), Scale bar: 100 µm.

2.3.2.2 Cell activity characterization of *in vitro* cultured cell encapsulated GelMA Constructs

It was previously reported that both pDE-HUVEC and pDM-HUVEC GelMA encapsulated cells exhibited highest metabolic activity in Gel 1 and Gel 3 respectively,

and exhibited only basal metabolic activity in GelMA Gel 2 (*99*). Because of the importance of MMP activity in dental cell differentiation and mineralized dentin and enamel matrix secretion (*104-106*), the MMP activity of *in vitro* cultured GelMA encapsulated cells were measured (Figure 2.2). Slightly increased MMP activity was found in pDE-HUVEC-encapsulated GelMA Gel 1 and Gel 3 constructs over time in culture (Figure 2.2). In contrast, GelMA Gel 2 encapsulated pDE-HUVECs exhibited a sharp decrease in MMP activity over time in culture (Figure 2.2). The pDM-HUVEC-encapsulated GelMA Gel 3 constructs exhibited increased MMP activity over time in culture, while pDM-HUVECs GelMA Gel 1 constructs exhibited decreased MMP activity over time in culture (Figure 2.2). pDM-HUVECs exhibited only basal level MMP activity in GelMA Gel 2 throughout the 4 weeks of *in vitro* culture. Together, these results indicate that GelMA Gels 1 and 3 supported cell attachment, morphology, and metabolic and MMP activities of encapsulated pDE-HUVEC and pDM HUVEC, respectively, while in contrast GelMA Gel 2 did not.

2.3.2.3 Capillary-like network formation within *in vitro* cultured GelMA constructs

A well-defined, functional vascularized network is required for the long term survival of bioengineered tissues, and for proper integration with the recipient host vasculature (*107, 108*). In natural tissues and organs, blood vessels are composed of a luminal endothelial cell layer, surrounded by a layer of smooth muscle cells (*89, 109-111*). Based on published reports that mesenchymal stem cells (MSCs) and endothelial cells exhibit the ability to self-organize into capillary-like networks after encapsulation in

GelMA hydrogel *in vitro* and *in vivo* (*89, 112*), immunofluorescent (IF) histochemical analyses was used to examine neo-vessel formation and organization within *in vitro*-cultured pDM-HUVEC-encapsulated GelMA constructs (Figure 2.3). An elaborate and well-defined capillary-like network formation was identified in pDM-HUVEC GelMA Gel 3 constructs (Figure 2.3), which appeared quite similar to vascular networks found in naturally formed dental pulp tissue (*79*). Confocal analyses revealed pDM and HUVEC cell organization within these networks (Figure 2.3). In contrast, capillary-like network formation was not observed in pDE-HUVEC constructs (Figure 2.3).

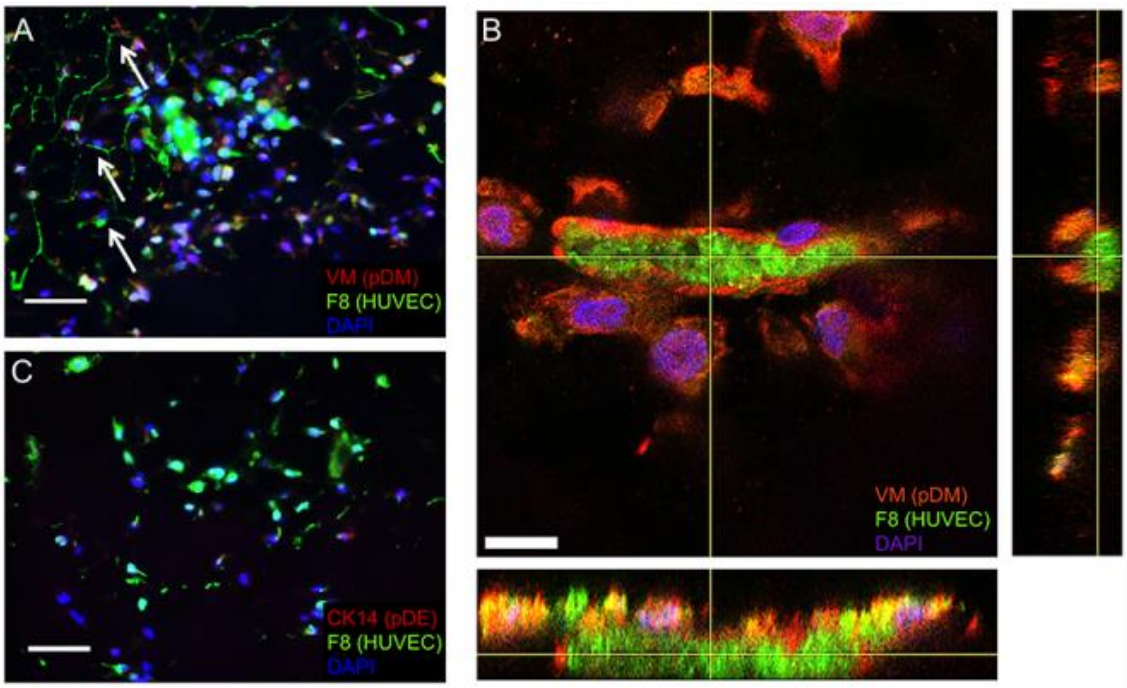

Figure 2.3. Capillary-like network formation within in vitro-cultured porcine dental mesenchymal (pDM)–human umbilical vein endothelial cells (HUVECs) gelatin methacrylate (GelMA) constructs. (a,b) pDM–HUVEC Gel 3 construct and (c) porcine dental epithelial (pDE)-HUVEC Gel 3 construct. Vascular network formation was observed in pDM–HUVEC GelMA Gel 3 constructs after 4 weeks of in vitro culture (a, arrows). Confocal analyses revealed organized pDM–HUVEC structures (b). No capillary-like formation was observed in pDE–HUVEC constructs (c). Bar: (a,c) 50 μm, (b) 10 μm

2.3.3 GelMA tooth bud constructs

Based on the promising preliminary *in vitro* analyses of DE-HUVECs and DM-HUVECs encapsulated within individual GelMA formulations, *in vitro* and *in vivo* analyses of 3D tooth bud GelMA constructs consisting of a GelMA Gel 1 encapsulated DE-HUVECs combined with GelMA Gel 3 encapsulated DM-HUVEC were performed (Figure 2.4). The resulting cell-seeded GelMA constructs were then cultured in osteogenic media for 2 weeks, and then either cultured *in vitro* for an additional 1 week or 6 weeks, or implanted subcutaneously into nude rat hosts *in vivo* for 1, 3 or 6 weeks (Figure 2.4).

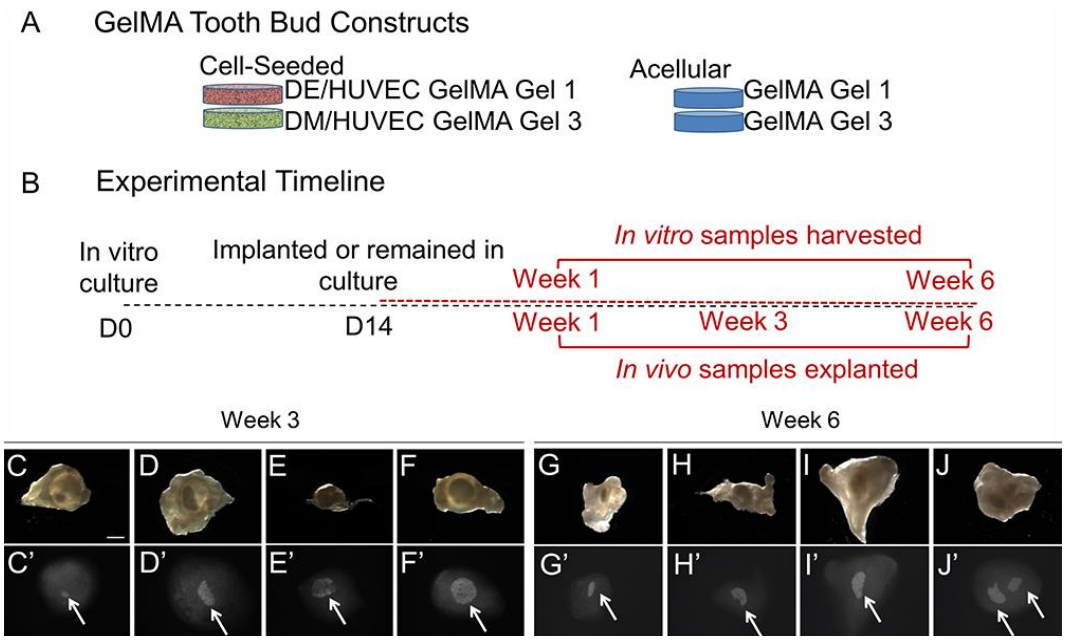

Figure 2.4. Parallel in vitro and in vivo bioengineered three-dimensional GelMA tooth bud constructs. (a) Schematic of construct fabrication. (b) Experimental timeline. (c–j) Harvested in vivo implanted GelMA tooth bud constructs. Representative bright field images of replicate in vivo GelMA constructs harvested after 3 weeks (c–f) or 6 weeks (g–j) implantation. (c'–j') Radiographic images of corresponding bright field images indicate mineralized tissue formation (arrows) in 3-week and 6-week constructs. Scale Bar: 2 mm. DE, dental epithelial cell; DM, dental mesenchymal cell; HUVEC, human umbilical vein endothelial cell.

2.3.3.1 In vitro cultured GelMA tooth bud constructs

Histological analyses of H&E-stained *in vitro*-cultured dental cell-HUVEC-encapsulated GelMA constructs revealed the presence of discrete and interconnected cell clusters throughout the constructs (Figure 2.5, arrows). In addition, H&E-stained dental cell-secreted extracellular matrix appeared to increase over time in *in vitro* culture, indicative of dental cell differentiation (Figure 2.5, arrowheads). The immunohistochemical analyses identified E-cadherin (Ecad)-expressing pDE cells, Vimentin (VM)-expressing pDM cells, and CD31 expressing HUVEC cell populations present throughout the *in vitro*-cultured constructs (Figure 2.5). Organized clusters of CD31 positive HUVECs increased in number and size over time in culture, and were localized throughout the constructs after 6 weeks of *in vitro* culture.

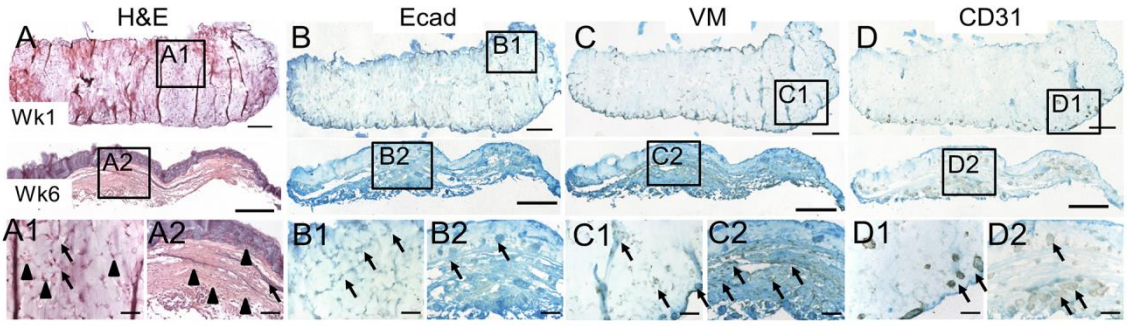

Figure 2.5. Cell distribution within *in vitro* cultured GelMA tooth bud constructs. (A) Distinct cellular networks and extracellular matrix secretion were evident in H&E stained sections of 1 and 6 week constructs (A1, A2 arrows). (B) Ecad expression in pDE cells predominantly localized within the upper portion of the construct (B1, B2 arrows). (C) VM expressing pDM cells were located predominantly in the bottom portion of the construct (C1, C2 arrows). (D) CD31 expressing HUVECs were present throughout the bilayered constructs (D1-D2). A1-D2 show higher magnifications of boxed regions of A-D. Scale bars: (A-D) 200 µm, (A1-D2) 50 µm.

Analyses of tooth and bone differentiation marker expression in sectioned *in vitro*-cultured GelMA constructs (Figure 2.6) revealed robust expression of the DM differentiation marker dentin sialophosphoprotein (DSPP) after both 1 week and 6 weeks of culture (Figure 2.6). The osteoblast differentiation marker osteocalcin (OC) was not detected in 1-week *in vitro* constructs, and only faintly detected in 6-week *in vitro*-cultured constructs (Figure 2.6). The pDE cell differentiation marker amelogenin (AM) was only faintly detected in both 1-week and 6-week *in vitro*-cultured constructs (Figure 2.6). Together, these results indicated that both pDE and pDM cells exhibited robust proliferation and dental cell differentiation marker expression in 3D tooth bud constructs after 6 weeks *in vitro* culture. In contrast, bone differentiation marker expression was weak, even after 6 weeks *in vitro* culture.

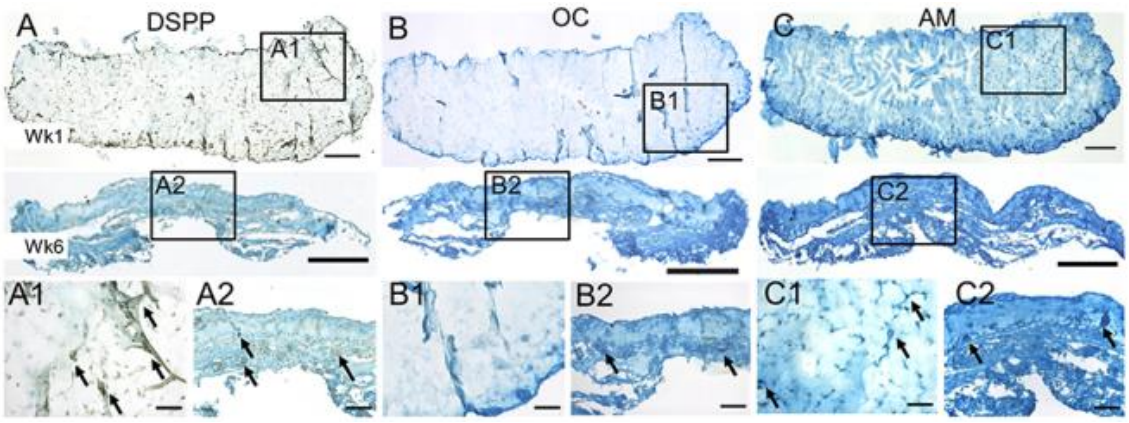

Figure 2.6. *In vitro* GelMA tooth bud constructs expressed bone and tooth specific proteins. (A-C) Robust DSPP expression was exhibited by 1 and 6 week *in vitro* cultured constructs (A1, A2 arrows). Faint OC expression was observed only at 6 weeks (B1, B2 arrows). AM expression was obvious at both 1 and 6 weeks (C1, C2 arrows). A1-C2 depict higher magnifications of boxed regions of A-C, respectively. Scale bar: (A-C) 200 μm, (A1-C2) 50 μm.

2.3.3.2 *In vivo* implanted GelMA tooth bud constructs

It was previously reported that *in vivo* implanted dental cell-encapsulated GelMA constructs exhibited hard tissue formation (*99*). In the present study, bright field and corresponding X-ray images of explanted *in vivo* constructs are provided (Figure 2.4). X-ray analyses revealed distinct areas of radio-opacity indicative of mineralized tissue formation (Figure 2.4). Mineralized tissues were present in 6/11 (55%) of the 3-week explants, and in 9/13 (69%) of 6-week explants. In many cases, mineralized tissue formation appeared to adopt the size and shape of the GelMA construct. All of the dental cell-encapsulated GelMA constructs grown *in vivo* for only 1 week, and all of the acellular GelMA constructs, appeared negative for mineralized tissue formation by X-ray. Following X-ray analyses, mineralized 3D tooth bud constructs were decalcified using weekly changes of decalcification solution, which were monitored for calcium precipitate (Figure 2.7). The majority of the 6-week *in vivo* constructs took longer to decalcify as compared to the 3-week i*n vivo* constructs, which was indicative of increased biomineralization of implanted constructs over time for *in vivo* growth.

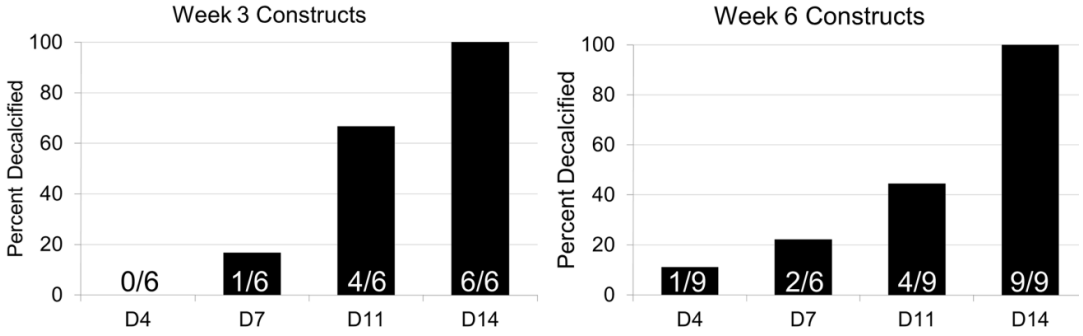

Figure 2.7. Decalcification times for mineralized *in vivo* GelMA tooth bud constructs. Construct decalcification was monitored at 4, 7, 11 and 14 days by ammonium oxalate-calcium precipitation (see Methods). Constructs exhibiting no precipitate after 20 minutes were classified as fully decalcified.

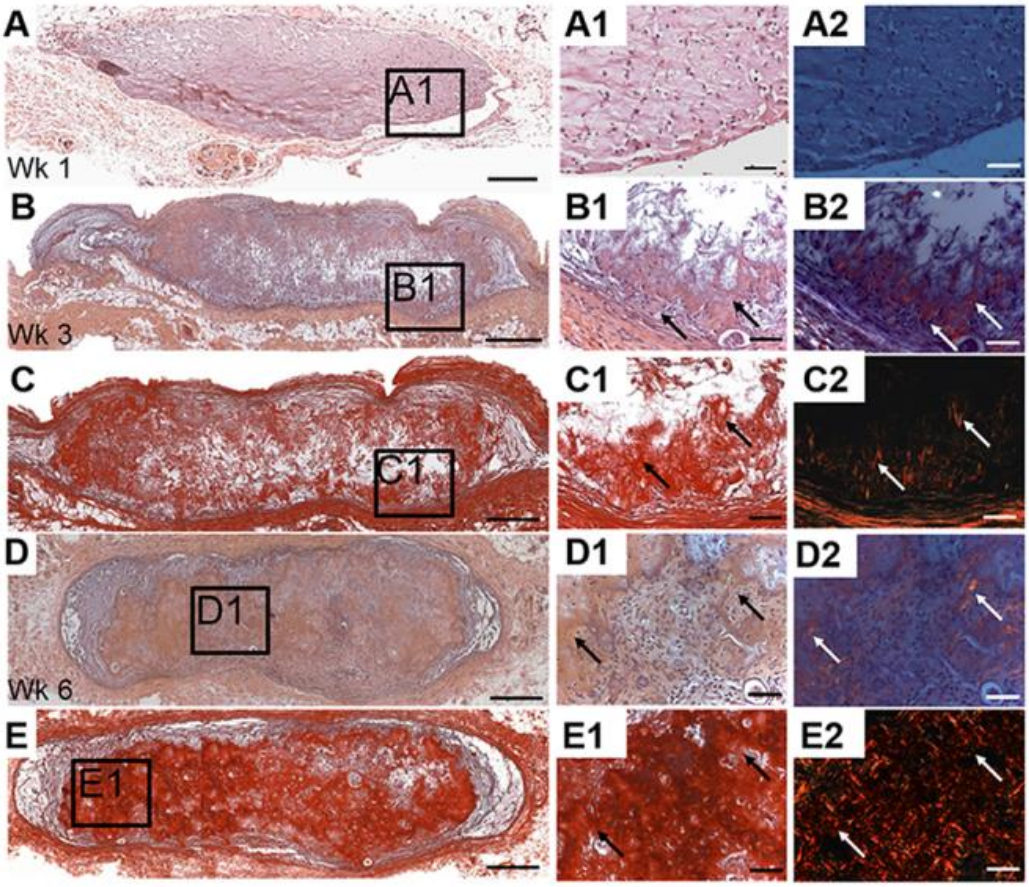

Figure 2.8. *In vivo* GelMA tooth bud constructs exhibited elaborate extracellular matrix formation. H&E stained paraffin embedded and sectioned GelMA constructs at (A) 1 week, (B) 3 weeks, and (D) 6 weeks. All constructs exhibited high cellularity. 3 and 6 week constructs exhibited bone-like tissue formation. Picrosirious Red (PSR) stained (C) 3 week and (E) 6 week explants revealed extensive extracellular matrix formation (arrows). A1-E1 depict higher magnification views of boxed regions in A-E, respectively. A2-B2 are polarized light images of A1-E1, revealing organized collagen formation within the GelMA constructs. Scale bars: (A-E) 200 µm, (A1-E1, A2-E2) 50 µm.

H&E-stained paraffin sectioned *in vivo* explants exhibited distinct GelMA tooth bud constructs surrounded by host tissue (Figure 2.8). The cellularity of the cell-seeded *in vivo* implanted constructs was observed to increase between 3 weeks and 6 weeks, and distinct neovascularization and the formation of bone-like tissues was observed

throughout the implants over time (Figure 2.8). Polarized light microscopy of H&E-stained sections revealed increased collagen matrix secretion by GelMA encapsulated cells over *in vivo* implantation time (Figure 2.8). Paraffin sectioned *in vivo* 3-week and 6-week explants were also examined using PicroSirious Red staining, which specifically detects collagen (red) under normal light microscopy, and under polarized light distinguishes between collagen type I (thick, yellow/orange) and collagen type III (thin, green). The *in vivo* 3-week and 6-week GelMA explants showed significant collagen content, consisting of both collagen type I and collagen type III fibers, indicative of newly formed collagen matrix (Figure 2.8). Collagen fiber alignment within the GelMA constructs appeared to be oriented perpendicular to the encapsulating host tissue (Figure 2.8), clearly defining collagen secretion by the encapsulated cell seeded GelMA constructs as opposed to that of rat host tissue.

Host red blood cells (RBCs) were observed in blood vessels located throughout the cell-seeded constructs (Figure 2.8, arrows). The presence of RBCs within the implanted constructs (Figure 2.9), which can

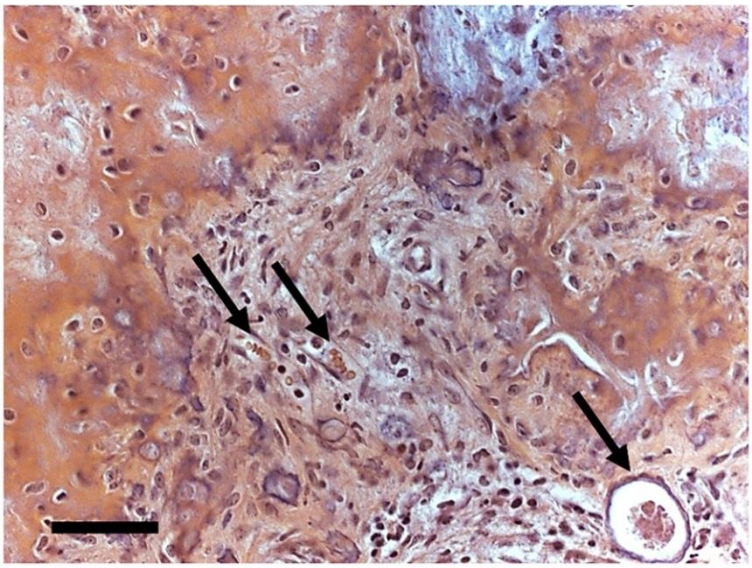

Figure 2.9. Functional vascularization of *in vivo* GelMA tooth bud constructs. Enlarged depiction of Figure 2.8, Panel D1, demonstrating host red blood cells present in bioengineered vasculature of *in vivo* GelMA tooth bud constructs (arrows). Scale bar: 50 µm.

only come from the host circulatory system, confirmed the functionality of bioengineered GelMA tooth bud vascular networks. Functional vasculature, defined as 'vasculature containing RBCs' (*89*, *113*), is required to support bioengineered tooth integration and growth after *in vivo* implantation. Immunohistochemistry was used to identify pDE, pDM, and HUVEC cell populations within *in vivo* implanted GelMA constructs (Figure 2.10). Ecad-positive pDE cells, VM-positive pDM cells, and CD31-positive HUVECS were clearly present throughout the entire construct in 1-, 3- and 6-week explants, indicating mixing of cells

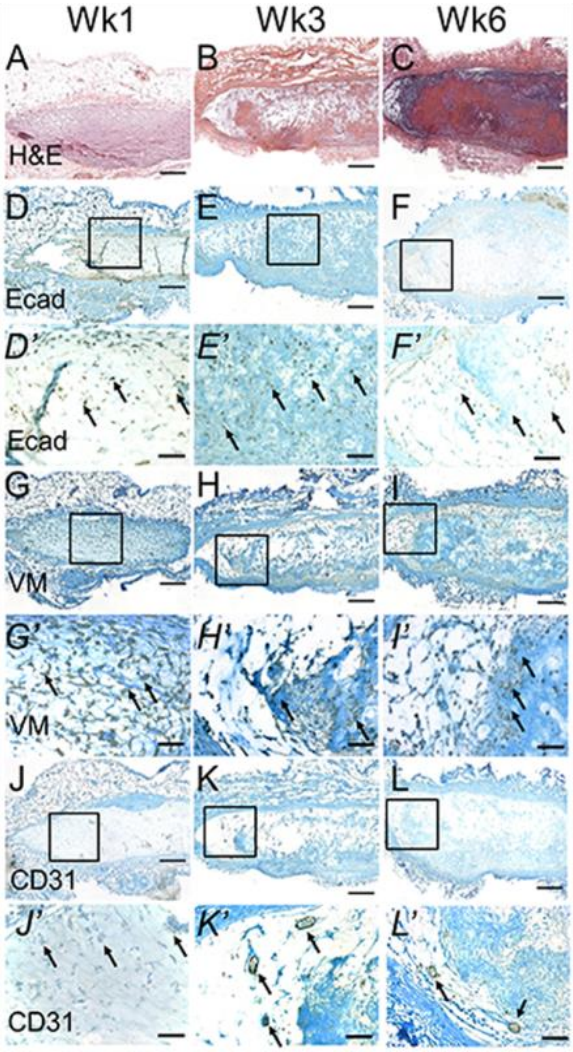

Figure 2.10. Dental cell and human umbilical Vein endothelial cell (HUVEC) distribution within *in vivo* gelatin methacrylate (GelMA) tooth bud constructs. (A-C) H&E staining revealed high cellularity and the development of bone-like tissue over time. Ecad expressing pDE cells (D-F, D'-F' arrows) and VM-expressing pDM cells (G-I, G'-I' arrows) were detected throughout the constructs. CD31 expressing HUVECs were also detected throughout the constructs (J-L, J'-L') and contributed to vascular networks in 3 and 6 week *in vitro* cultured constructs (K', L' arrows). D'-I' are higher magnifications of boxed regions in D-I. Scale bars: (A-I) 200 μm, (D'-I') 50 μm.

throughout the construct (Figure 2.10). Organized CD31-expressing neovasculature was apparent after 3 weeks and 6 weeks *in vivo* growth (Figure 2.10). As the CD31 antibody used in these analyses is human specific (Figure 2.11), these results indicated GelMA encapsulated HUVEC (as opposed to host cell) contribution to the neovasculature that formed within GelMA tooth bud constructs.

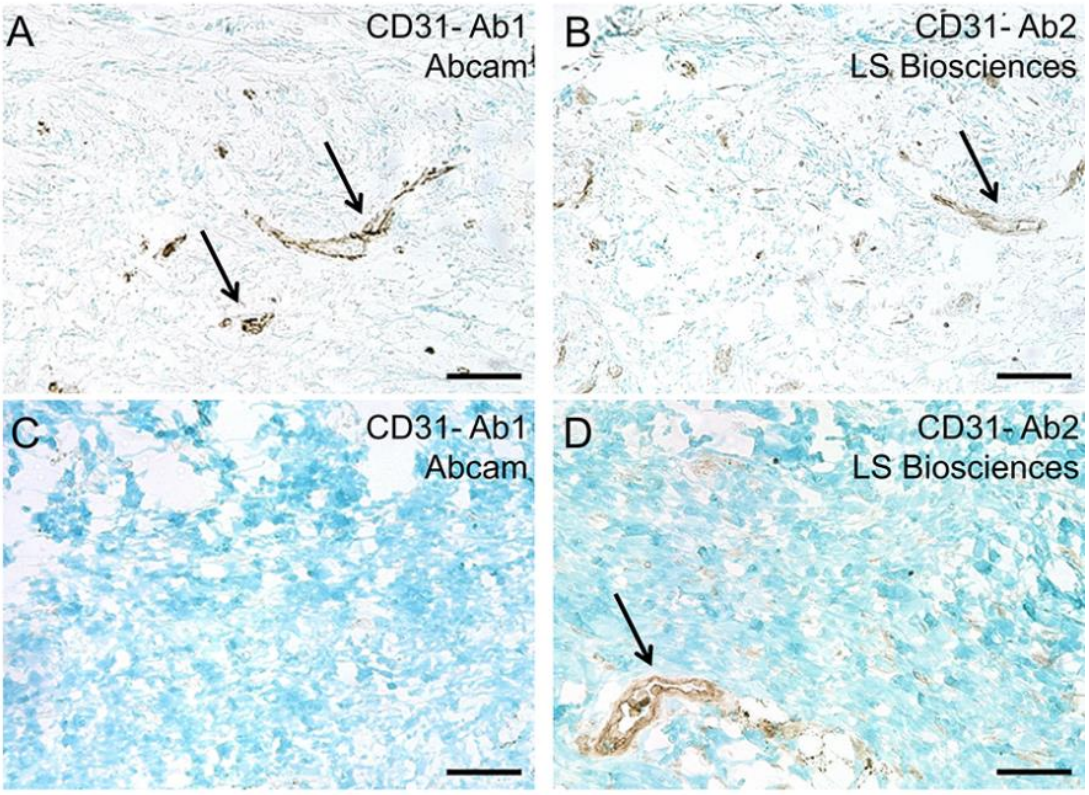

Figure 2.11. Specificity of α-CD31 antibodies. (A, B) Human gingival and (C, D) rat dermal paraffin sections were stained with the human specific CD31 antibody (Abcam) (Ab1) and the human/mouse specific CD31 antibody (Lifespan Biosciences) (Ab2). Ab1 identified endothelial cells in human gingiva (A, arrows), but not in rat dermal tissue (C). Ab2 recognized both human and rat endothelial cells (B, D arrows). Ab1, the human specific CD31 antibody (Abcam), was therefore used to characterize HUVEC contribution to the vasculature found in bioengineered constructs. Scale bar:

Dental cell differentiation marker expression within harvested *in vivo* GelMA constructs was examined next (Figure 2.12). Distinct and robust DSPP and OC expression was detected in sectioned 3-week and 6-week *in vivo* implanted constructs, which was indicative of both DM cell-derived odontoblast and osteoblast cell differentiation (Figure 2.12). This observation supports previous reports from this group (*44, 53, 54*) and those of others (*114, 115*), which have shown that DM cells exhibit the capacity to develop into osteodentin producing cells that can express both DSPP and OC.

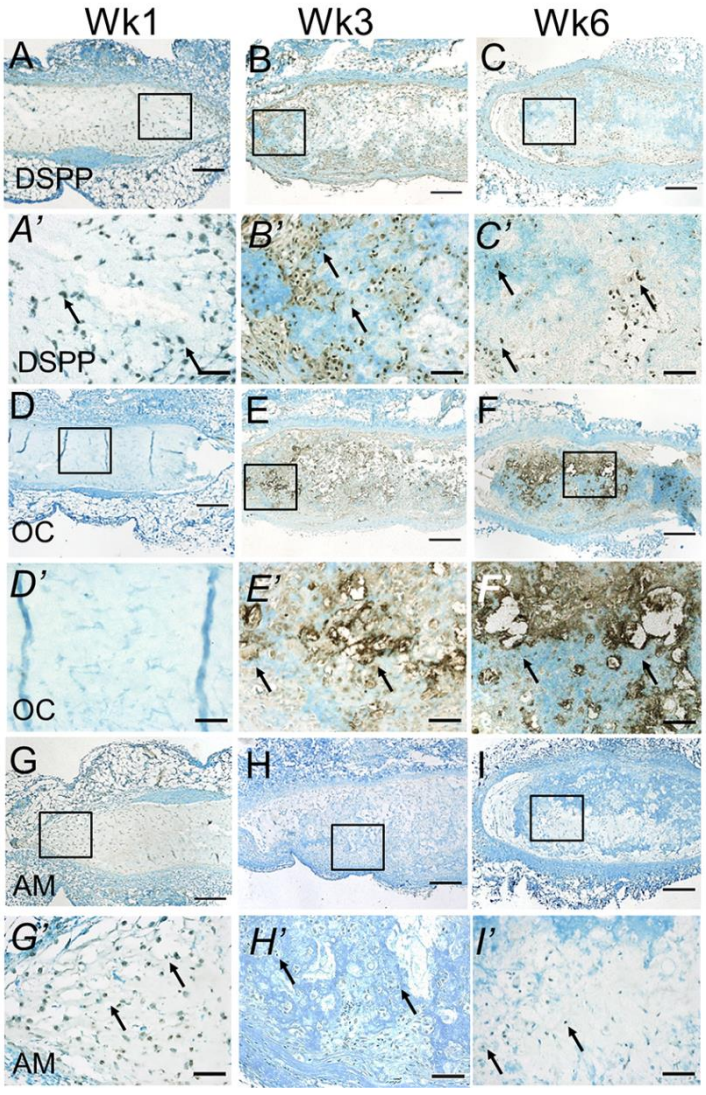

Figure 2.12. Figure 5. Dental cell differentiation within in vivo gelatin methacrylate (GelMA) tooth bud constructs. **A**–I Immunohistochemical analyses of tooth and bone specific markers in 1-, 3- and 6-week *in vivo* constructs. The odontoblast differentiation marker dentin sialophosphoprotein (DSPP) was detected throughout the constructs at each time-point (A–C, A'–C'). Odontoblast/ osteoblast differentiation marker osteocalcin (OC) expression increased over time *in vivo* (d–f, d'–f'). Ameloblast differentiation marker amelogenin (AM) was detected throughout the constructs at all times (G–I, G'–I'). (A'–I') Higher magnification images of boxed regions in A–I. Bar: (A–I) 200 μm, (A'–I') 50 μm

Similarly, AM expression was clearly observed in 1-, 3- and 6-week *in vivo* tooth bud constructs, which is indicative of DE cell-derived ameloblast differentiation (Figure 2.12). Together, these results support the successful generation of 3D biomimetic tooth constructs exhibiting mineralized osteodentin-like and enamel matrix formation.

2.4 Discussion

The ability to successfully create bioengineered replacement teeth that resemble and function as well as natural teeth, would provide distinct advantages over currently used synthetic dental implants (*4*). The present study has described the design and characterization of dental and endothelial cell encapsulated GelMA constructs as 3D biomimetic tooth bud models. Encapsulated cell behavior is highly influenced by the architecture and mechanical properties of the scaffold (*45, 116*), which in turn direct cell differentiation, fate and function (*45, 117-121*). Based on previous reports, we sought to identify GelMA formulas that exhibited elastic moduli similar to those of natural tooth bud enamel organ and pulp organ tissues. The FV-AFM analyses of the elastic moduli of dental cell encapsulated GelMA Gel 3 constructs closely matched that of fresh pDM tissue. In contrast, dental cell seeded GelMA Gel 1 constructs were below the level of detection by FV-AFM, as was natural tooth bud enamel organ tissue (Figure 2.1). Characterization of *in vitro*-cultured individually encapsulated pDE-HUVEC and pDM-HUVEC GelMA constructs provided insight to cellular morphology and metabolic activity in each GelMA formula. Based on the results of the present study, pDM-HUVEC cell-seeded GelMA Gel 3, and pDE-HUVEC cell-seeded GelMA Gel 1 were selected to

create 3D biomimetic tooth bud constructs. The GelMA Gel 2 formula did not support cell proliferation or metabolic activity of encapsulated cells, likely because of toxicity introduced by high photoinitiator concentration.

The design of our fabricated 3D biomimetic tooth bud constructs was intended to facilitate cross-talk between DE-DE cells, DM-DM cells, and between adjacent pDM-HUVEC and pDE-HUVEC cell layers, while at the same time maintaining distinct pulp organ and enamel organ, respectively. However, subsequent immunohistochemical analysis of harvested *in vitro*-cultured and *in vivo*-grown implants showed that pDE and pDM cells were not maintained in separate layers, but rather were present throughout the constructs even after only 1 week of culture and/or implantation. These results likely indicate mixing of the dental cell/GelMA solutions prior to photocrosslinking. Future studies will employ successive photocrosslinking of individual cell-seeded GelMA layers to avoid mixing.

Another limitation of this bioengineered 3D tooth bud model, and a consequence of the above mentioned cell mixing, is that no distinct enamel or dentin layers were observed. Sequential photo-crosslinking combined with the inclusion of additional dental cell differentiation growth factors will likely improve this model to better support dentin and enamel formation. In addition, the inclusion of bioreactor culture conditions that can deliver mechanical stimulation, followed by longer *in vivo* implantation times, may also help to achieve our goal to create functional, biological tooth substitutes.

It is notable that our *in vivo*-cultured biomimetic 3D tooth bud constructs formed robust mineralized tissues that largely adopted the size and shape of the original

constructs – an important criterion for an effective biomimetic tooth bud model. In addition, 3D dental cell encapsulated GelMA tooth bud constructs expressed dental epithelial and dental mesenchymal differentiation markers indicative of ameloblast and odontoblast specific cell differentiation, respectively. Also noteworthy is the fact that *in vivo* implanted dental cell-encapsulated GelMA tooth bud constructs exhibited functional vascularization, demonstrated by CD31-expressing HUVEC derived neovasculature and the presence of circulating host RBCs (Figure 2.9). Furthermore, bioengineered capillary-like networks present in both *in vitro* cultured and *in vivo* implanted constructs resembled natural neovasculature organization (Figure 2.13). Together, these results suggest the potential to eventually create viable, vascularized, functional bioengineered tooth replacements.

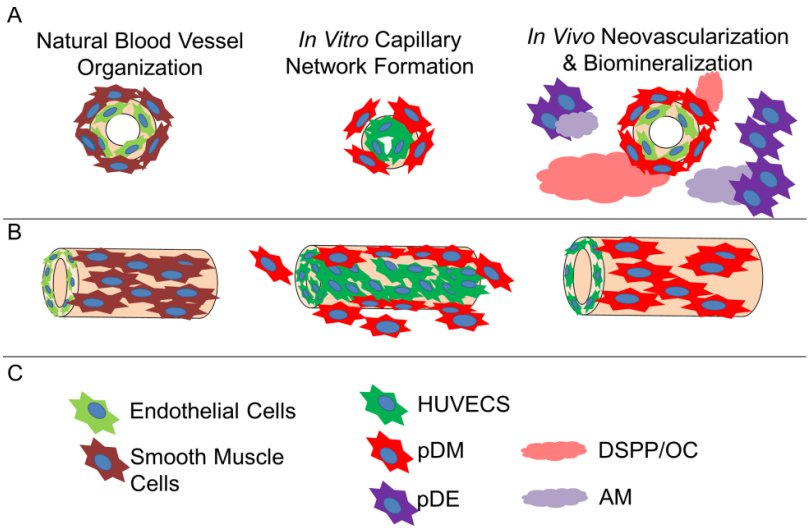

Figure 2.13. Schematic of bioengineered neovascular formation in gelatin methacrylate (GelMA) tooth bud constructs. (a) Cross-sectional and (b) longitudinal schematic along with a (c) color-coded key depicting the organization ofnormal blood vessel, in vitro-cultured GelMA construct capillary network formation, and neovascularization and mineralization of in vivo implanted GelMA constructs. AM, amelogenin; DSPP, dentin sialophosphoprotein; HUVEC, human umbilical vein endothelial cell; OC, osteocalcin; pDE, porcine dental epithelial cell; pDM, porcine dental mesenchymal cell

In conclusion, these results presented here validate GelMA hydrogel constructs as promising scaffold materials for whole-tooth engineering and craniofacial reconstruction. This appears to be the first study to successfully demonstrate that dental cell-encapsulated GelMA hydrogels can be used to create bioengineered 3D tooth buds that support dental cell differentiation, functional neovasculature and dental tissue derived mineralized tissue formation. Future studies will focus on refining our 3D biomimetic tooth bud model to better facilitate DE and DM cell interactions, while preserving DE- and DM-derived enamel organ and pulp organ tissue formation and differentiation. Biomimetic 3D GelMA tooth bud constructs provide a promising model for the eventual development of functional, bioengineered replacement teeth of specified size and shape.

Chapter 3: Bioengineered Teeth Exhibit Characteristic Features of Natural Teeth[3]

[3] Smith EE, Angstadt S, Monteiro N, Zhang W, Khademhosseini A, Yelick PC. Submitted to *Journal of Dental Research*, 01/24/2018. Videos are available in the online version.

3.1 Introduction

Dental implants are synthetic and therefore lack most features of natural teeth including vascularized pulp, periodontal ligament and proprioception. Synthetic dental implants are susceptible to peri-implantitis, gingival recession, and bone resorption at the implant site leading to implant failure (*2, 122-124*). To create vitalized teeth for human tooth replacement, bioengineered tooth regeneration has emerged as an innovative field of Translational Dentistry. Studies have shown that post-natal dental stem cells (DSCs) retain the ability to form small, anatomically correct whole tooth crowns in *in vivo* rat and mini pig animal models, supporting the feasibility of this approach (*17, 18, 49*).

Currently, a variety of biodegradable scaffolds are being tested for utility in whole tooth regeneration therapies (*48, 125*). In particular, Gelatin methacryloyl (GelMA) hydrogel scaffolds were shown to support DSCs and human umbilical vein endothelial cells (HUVECs) differentiation into mineralized dental tissues of specified size and shape (*126*). To improve upon this model, here we investigated three ways to improve GelMA tooth bud constructs to facilitate their use in humans. First, we tested whether sequentially photo-crosslinking GelMA bilayers would better maintain distinct dental epithelial (DE) and dental mesenchymal (DM) cell layers. Next, to optimize cell seeding densities (*127-129*), we compared dental cell differentiation in constructs created using our original cell seeding density to those using doubled and tripled cell seeding densities (3.0×10^7, 6.0×10^7, 9.0×10^7 cells/mL). Lastly, we tested whether extended culture time in normal growth media, prior to culture in osteogenic differentiation media, resulted in improved tooth bud construct cellularity and mineralized dental tissue formation.

3.2 Materials and Methods

3.2.1 Dental and Endothelial Cell Culture

DE and DM cells were isolated from porcine tooth buds and cultured as previously described (*126*). Human Umbilical Vein Endothelial Cells (HUVECs) (PCS100010, ATCC, Manassas, VA) were grown in vascular basal media (PCS100030, ATCC) with VEGF growth kit (PCS10004, ATCC). All cells were expanded in 5% CO2, at 37^0C and cryopreserved in 10% DMSO until use.

3.2.2 Fabrication of 3D GelMA Hydrogel Tooth Bud Constructs

Cells were encapsulated within GelMA hydrogel at densities of 3.0 x 10^7, 6.0 x 10^7, or 9.0 x 10^7 total cells/mL (1X, 2X or 3X, respectively). DM:HUVECs (1:1) were pelleted and resuspended in 5% GelMA with 0.1% photoinitiator (PI, Irgacure2959, Sigma, St. Louis, MO), aliquoted (20 uL) into 6 mm diameter circular PDMS molds in 24 well plate wells, and photocrosslinked for 18 seconds using an Omnicure S200 (Lumen Dynamics Group Inc., Mississauga ON, Canada). DE:HUVECs (1:1) were pelleted, resuspended in 3% GelMA with 0.1% PI, pipetted (20 uL) on top of each photopolymerized DM-HUVEC 5% GelMA layer and photocrosslinked for 12 seconds. The resulting bilayered tooth bud constructs were cultured in normal growth media [DMEM/F12: LCH8: vascular basal media (1:1:1)], supplemented with 10% FBS, 1% Pen-Strep, 0.5 µg/mL epinephrine, 25 µg/mL ascorbic acid, 2 mM glutamax, and endothelial cell growth kit (ATCC PCS-999-003), for 1 or 7 day(s), followed by 7 day

culture in odontogenic media (OM, 1:1:1 culture media + 100 nM Dexamethasone, 10mM beta glycerol phosphate, 50 µg/mL ascorbic acid).

3.2.3 Live/Dead Assay

The Live/Dead assay (Molecular Probes, Eugene, OR) was used to determine cell viability in *in vitro* tooth bud constructs as recommended.

3.2.4 In Vivo Implantation of Tooth Bud Constructs

Animal surgeries were performed using Tufts University IACUC approved protocols. Replicate (4) tooth bud constructs were randomly implanted subcutaneously on the backs of 5-week-old female Rowett Nude rats (RNU, Charles River Laboratories, Wilmington, MA) and grown for 2 or 4 weeks.

3.2.5 Tooth Bud Construct Harvest and Micro-CT Analysis

Harvested constructs were fixed overnight in 10% formalin, washed in PBS, and imaged using a Skyscan 1176 *In Vivo* Micro-CT (Bruker, Billerica, MA). Reconstructions and analyses were performed using Skyscan NRecon, Bruker-microCT CT Analyzer software (Bruker MicoCT, Kontich, Belgium) and Avizo software (FEI, Hillsboro, Oregon).

3.2.6 Histological and Immunohistochemical (IHC) analyses.

Decalcified constructs were paraffin embedded were sectioned at 6 µm, and stained using Hematoxylin and Eosin (H&E). IHC was performed as described (Smith et al., 2016) using primary antibodies: mouse anti-vimentin (sc-6260, 1:4000, Santa Cruz

Biotechnology, Dallas, Texas); rabbit anti-Ecadherin (ABIN1858334, 1:40, Antibodies Online, Atlanta, GA); mouse anti-hCD31 (ab187377, 1:20, Abcam, Cambridge, MA); rabbit anti-hCD31 (LS-B5577, 1:200, LifeSpan BioSciences, Seattle WA; mouse anti-Osteocalcin (ab13418, 1:100, Abcam); rabbit anti-Dentin Sialophosphoprotein (GTX60194, 1:150, Genetex, Irvine, CA); rabbit anti-Amelogenin (ABT260, 1:500, Millipore, Billerica, MA); rabbit anti-Ki67 (ab15580, 1:200, Abcam); and rabbit anti-Caspase-3 (ab4051, 1:20, Abcam); followed by secondary antibodyies anti-mouse IgG (711-065-150, 1:500, Jackson ImmunoResearch) or anti-rabbit IgG (711-065-152, 1:500, Jackson ImmunoResearch Laboratories, West Grove, PA). Sections were then treated with ABC reagent (PK-4000, Vector Laboratories) and DAB (D4293, Sigma, St. Louis, MO), and counterstained with 0.1% fast green (F7252, Sigma).

Immunofluorescent (IF) analyses were performed as published (Smith et al., 2016) using primary antibodies: mouse anti-Fibroblastic Growth Factor 3 (ab10830 1:50-1:100, Abcam); rabbit anti-Sonic Hedgehog (sc-9024, 1:50, Santa Cruz Biotechnology); mouse anti-Beta catenin (LS-C172582, 1:50, LifeSpan BoiScience); rabbit anti-Ecadherin (1:40, ABIN1858334, Antibodies online); mouse anti-Sox2 (1:50, ab79351, Abcam), rabbit anti-Ki67 (ab15580, 1:50, Abcam); mouse anti-Fibrillin (1:50, gift); rabbit Fibrillin 2 (1:100, gift); mouse anti anti-Dentin sialophosphoprotein (SC-73632, 1:100, Santa Cruz Biotechnology); rabbit anti osteocalcin (1:50, gift) and rabbit anti Amelogenin (ABT260, 1:100, Millipore). Secondary antibodies (Invitrogen, Carlsbad, CA) included: goat anti-mouse IgG-Alexa Fluor 568 (A-11031, 1:100); goat-rabbit IgG-Alexa Fluor 488 (A-11034, 1:100); goat anti-mouse IgG-Alexa Fluor 488 (A-11001, 1:100); and goat-rabbit

IgG-Alexa Fluor 568 (A-11011, 1:100).

3.3 Results

3.3.1 Initial cell seeding density positively correlated with *in vitro* cultured tooth bud construct cell density

Bioengineered tooth bud constructs were fabricated consisting of a dental epithelial (DE) and HUVEC cell layer, and a dental mesenchymal (DM) and HUVEC cell layer, at three cell seeding densities – 1X, 2X, and 3X - as indicated in Materials and Methods and (Figure 3.1).

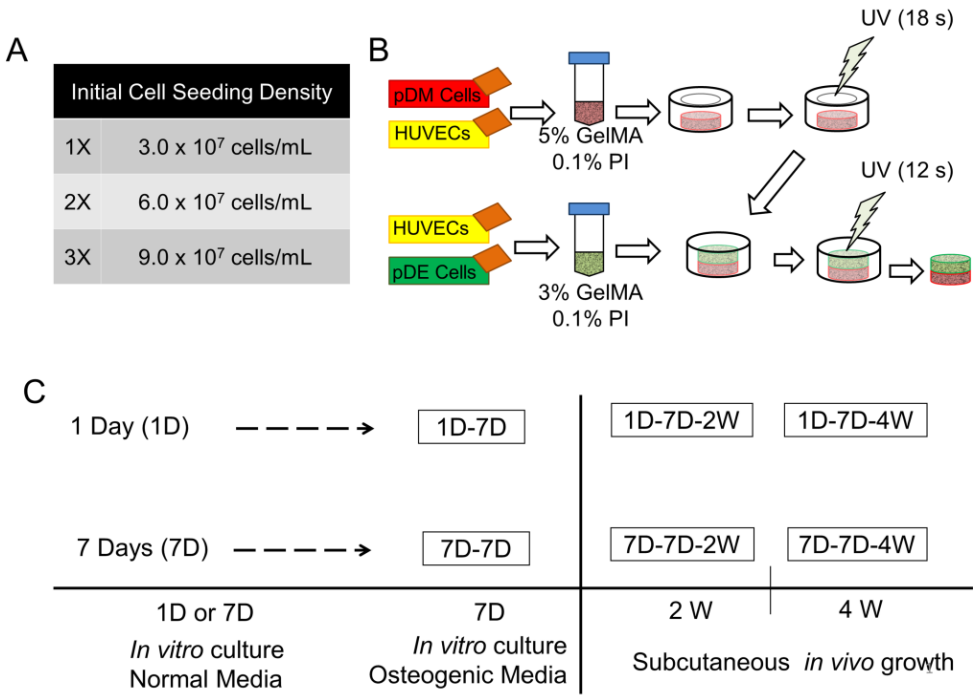

Figure 3.1. Bioengineered Tooth Bud Construct Fabrication. Schematic of tooth bud construct fabrication. **(A)** Cell seeding densities. **(B)** Preparation of 5% GelMA encapsulated DM cells/HUVECs, and 3% GelMA encapsulated DE cells/HUVECs. Sequential photo-crosslinking method. **(C)** Timeline for *in vitro* cultured and *in vivo* implanted tooth bud constructs. Constructs were grown in normal media for 1 or 7 day(s) (1D, 7D), and then in osteogenic for an additional 7 days (7D), creating 1D-7D and 7D-7D constructs. Constructs were implanted subcutaneously for 2 weeks (2W) or 4 weeks (4W).

Sequential photo-polymerization of the DM/HUVEC GelMA layer, and then the DE/HUVEC cell GelMA layer, was used to create bi-layered constructs (Figure 3.1). The resulting tooth bud constructs were cultured in normal media for 1 day (1D) or 7 days (7D), followed by 7D culture in osteogenic media (OM) (1D-7D, and 7D-7D, respectively) (Figure 3.1), and then implanted subcutaneously for 2 or 4 weeks (Figure 3.1).

H&E stained paraffin sectioned *in vitro* cultured constructs showed that sequential photo-crosslinking resulted in distinct bilayer formation (Figure 3.2). Furthermore, the initial cell seeding densities positively correlated with cell density of all *in vitro* cultured constructs (Figure 3.2). Distinct epithelial rosette-like structures formed in both 1D-7D and 7D-7D constructs (Figure 3.2, arrows), which resembled those present in embryonic and adult tissue development, including developing tooth buds (*130-133*). Live/Dead staining revealed high cell viability in all 1D-7D constructs and reduced cell viability in 7D-7D constructs (Figure 3.2). Cell proliferation, assessed via Ki67 expression, increased with cell seeding density in 1D-7D constructs (Figure 3.2), but appeared similar at all 7D-7D cell seeding densities (Figure 3.2). Apoptosis, assessed via Caspase 3 expression, was low in 1D-7D constructs as compared to 7D-7D constructs (Figure 3.2). Together, these results showed that *in vitro* cultured 1D-7D constructs exhibited robust cell proliferation and low levels of apoptosis, while 7D-7D culture conditions exhibited relatively reduced cell densities, reduced cell proliferation, and increased levels of apoptosis.

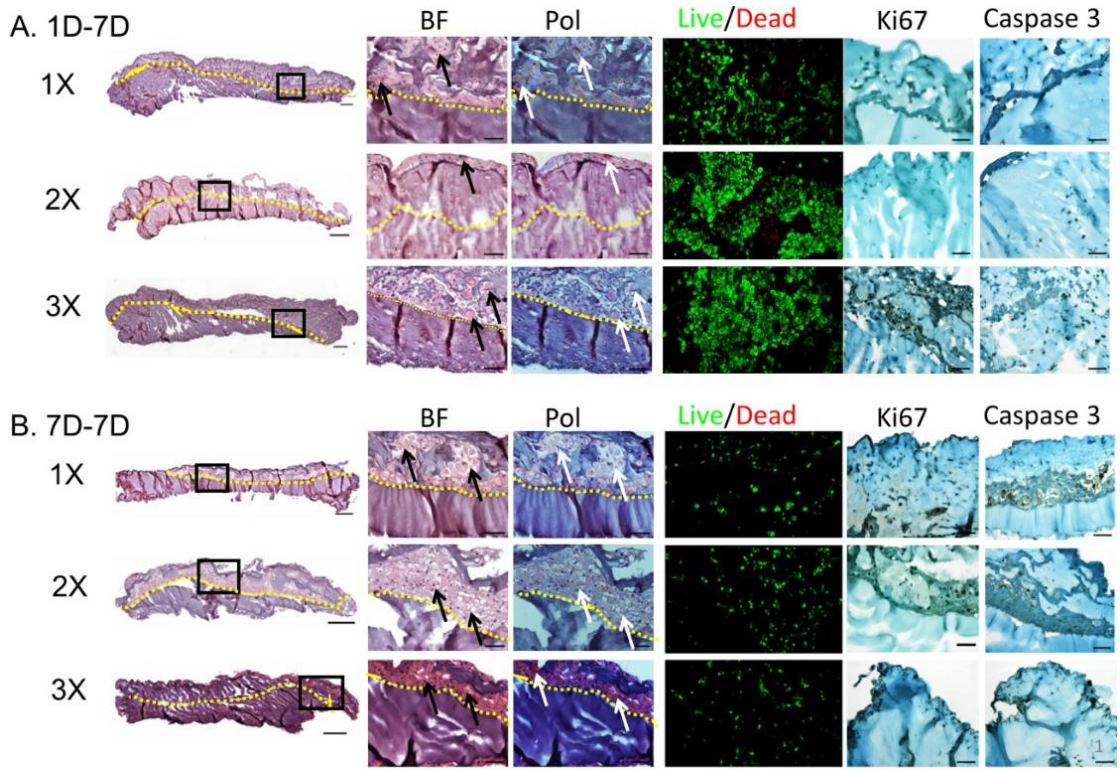

Figure 3.2. Initial Cell Seeding Density Positively Correlated with *In Vitro* Cultured Construct Cell Density. H&E staining, Live/Dead analyses, and immunostained paraffin sections of **(A)** 1D-7D and **(B)** 7D-7D *in vitro* cultured constructs. **(A)** Increased initial cell seeding densities in 1D-7D *in vitro* cultured constructs trended toward increased cell viability, and proliferation (Ki67), and stable levels of apoptosis (Caspase3). **(B)** Cell density, viability, and proliferation appeared comparable among all of the 7D-7D constructs, but was decreased relative to 1D-7D constructs. Apoptosis was increased in 7D-7D constructs as compared to 1D-7D constructs. Rosette-like structures were identified in 1D-7D constructs, and were increased in size in 7D-7D constructs (arrows). Scale bars: 200 μm (A, B), 50 μm (A1, A2, B1, B2).

3.3.2 Dental cell localization and differentiation in *in vitro* constructs

Distinct E-Cadherin (ECAD)-expressing DE cells were restricted to the top layer of bilayered tooth bud constructs, Vimentin (VM)-expressing DM cells were located in the bottom layer of all constructs, and CD31 positive neovascular-like structures were present throughout both layers of all *in vitro* cultured constructs (Figure 3.3). CD31

expression in 7D-7D cultured constructs exhibited was consistently more robust as compared to the 1D-7D constructs, suggesting that extended culture time in normal media facilitated HUVEC proliferation.

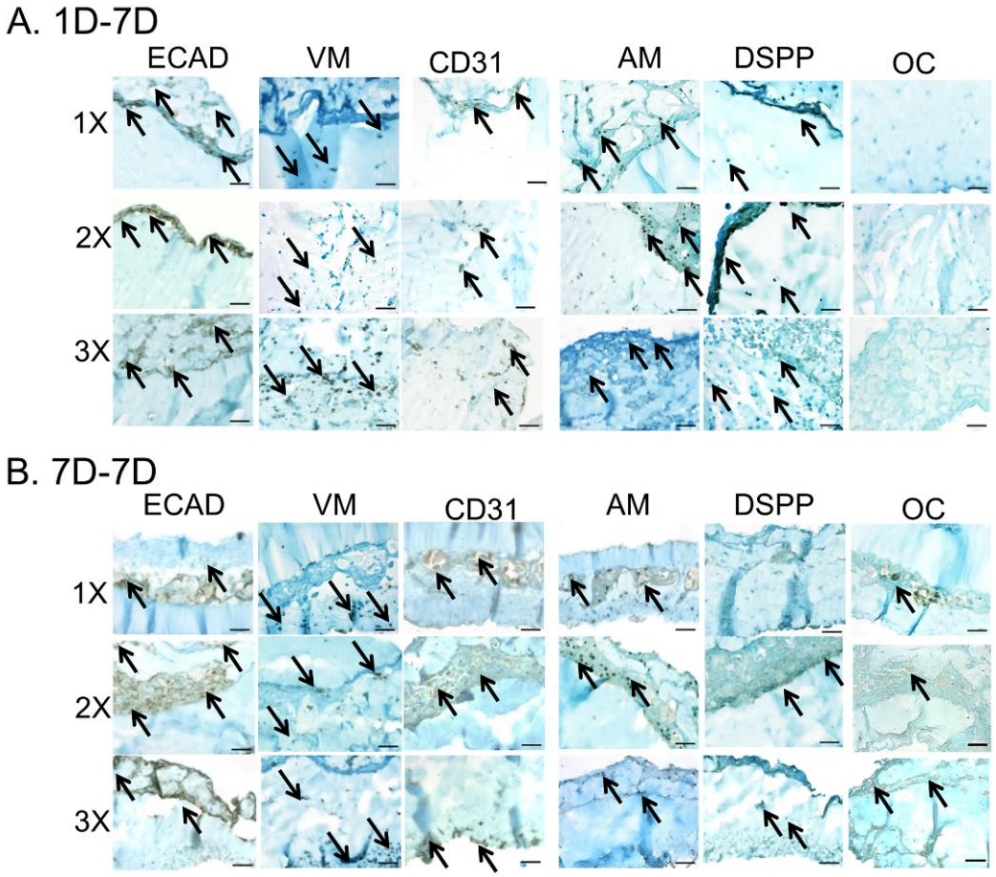

Figure 3.3. Cell Type Specific Localization and Differentiation in *In Vitro* Constructs. 1D-7D **(A)** and 7D-7D **(B)** *in vitro* cultured constructs. ECAD positive DE cells localized to the top layer, VM positive DM cells localized to the bottom layer, and CD31 positive vascular-like structures were present throughout both layers of *in vitro* cultured 1D-7D **(A)** and 7D-7D **(B)** constructs. AM expression was detected in the top DE layer of all 1D-7D **(A)** and 7D-7D **(B)** constructs. DSPP was detected at the DE/DM bilayer interface and throughout the DM layer of all 1D-7D constructs **(A)**, and at the DE/DM cell layer interface and DM layer of 2X, 3X 7D-7D constructs. Reduced DSPP expression was observed in 1X, 7D-7D constructs **(B)**. Osteocalcin (OC) expression was not detected in any of the *in vitro* cultured 1D-7D constructs **(A)**, but was robustly expressed in 1X 7D-7D constructs, and weakly expressed in 7D-7D 2X and 3X constructs **(B)**. Scale bar: 50 μm. Abbreviations: AM, amelogenin; DE, dental epithelial; DM, dental mesenchymal; DSPP, dentin sialophosphoprotein; ECAD, E-cadherin; HUVEC, human umbilical vein cells; OC, osteocalcin.

The DE cell differentiation marker Amelogenin (AM) was detected throughout the DE/HUVEC layers of all 1D-7D and 7D-7D *in vitro* constructs (Figure 3.3). The DM cell differentiation marker Dentin Sialophosphoprotein (DSPP) was strongly expressed at the DE/DM interface and throughout the DM cell layer of 1D-7D 1X and 2X constructs, and weakly expressed in 3X constructs. Relatively faint DSPP expression was observed in 7D-7D 2X and 3X constructs, with no detectable expression in 1X constructs (Figure 3.3). OC was not detected in any of the 1D-7D *in vitro* cultured constructs, but was detected in the 1X, 2X, and 3X 7D-7D constructs (Figure 3.3). Therefore, DE differentiation into pre-ameloblasts was supported by both 1D-7D and 7D-7D conditions at all cell densities, and that DSPP expressing pre-odontoblasts, and not OC expressing osteoblasts, were observed in 1X and 2X 1D-7D conditions. Both osteoblast and pre-odontoblast differentiation were observed in 2X and 3X 7D-7D constructs.

3.3.3 Classification of *in vivo* grown tooth bud constructs

Two and 4 week *in vivo* harvested constructs were analizyed by micro-CT and then demineralized, paraffin embedded and sectioned. All *in vivo* implanted 1D-7D and 7D-7D constructs exhibited well-defined bilayers (Figure 3.4-3.7). Micro-CT and histological analyses were used to classify the constructs into 4 types: 1) mineralized DE rosette containing (MR); 2) mineralized non-rosette containing (M); 3) non-mineralized rosette containing (R); and 4) non-mineralized non-rosette containing (Table 3.1, Figures 3.4-3.7).

In Vivo		Mineralized Rosette	Mineralized Non-rosette	Non-mineralized Rosette	Non-mineralized Non-rosette
1D-7D 2W	1X	0/3	0/3	0/3	3/3
	2X	0/3	0/3	2/3	1/3
	3X	1/4	0/4	1/4	2/4
Total		**10% (1/10)**	**0% (0/10)**	**30% (3/10)**	**60% (6/10)**
7D-7D 2W	1X	0/3	0/3	1/3	2/3
	2X	0/2	0/2	2/2	0/2
	3X	0/3	0/3	3/3	0/3
Total		**0% (0/8)**	**0% (0/8)**	**75% (6/8)**	**25% (2/8)**
1D-7D 4W	1X	0/4	1/4	0/4	3/4
	2X	0/3	2/3	0/3	1/3
	3X	1/3	0/3	1/3	1/3
Total		**10% (1/10)**	**30% (3/10)**	**10% (1/10)**	**50% (5/10)**
7D-7D 4W	1X	0/3	1/3	0/3	2/3
	2X	0/3	1/3	0/3	2/3
	3X	0/1	0/1	0/1	1/1
Total		**0% (0/7)**	**29% (2/7)**	**0% (0/7)**	**71% (5/7)**

Table 3.1. Classification of *In Vivo* Grown Tooth Bud Constructs. Constructs were classified into 4 groups including: 1) mineralized rosette; 2) mineralized non-rosette; 3) non-mineralized rosette; and 4) non-mineralized non-rosette. 2W and 4W constructs are further classified as1D-7D and 7D-7D *in vitro* culture conditions, and by initial cell seeding densities. Mineralized tissue with rosette-like structures were only found in 1D-7D, 3X constructs at 2W and 4W (shaded purple). Mineralized non-rosette constructs were most common at 4W (shaded red). Non-mineralized rosettes occurred most frequently in 2W constructs (shaded blue), predominantly in 7D-7D constructs. In general, non-mineralized, non-rosette constructs comprised the majority of all of the constructs (green shade), except for the 2W 7D-7D constructs, which mostly contained non-mineralized rosette.

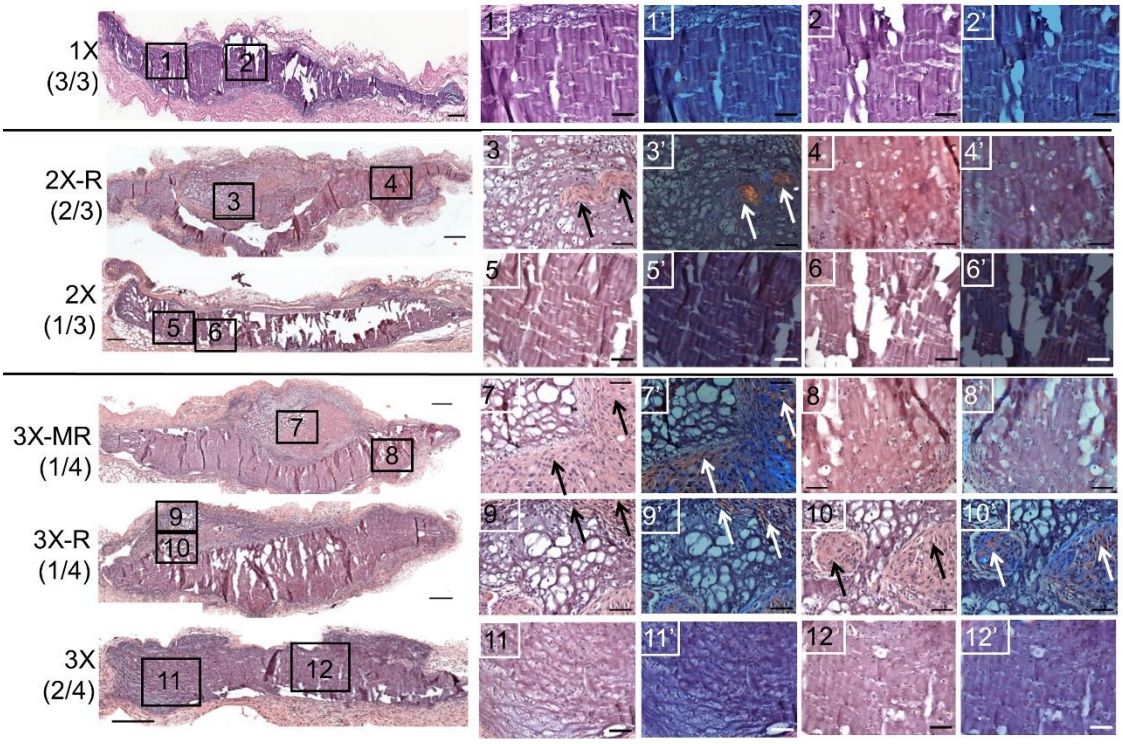

Figure 3.4. 2W, 1D-7D *In Vivo* Constructs. All 2W, 1D-7D 1X, 2X, 3X constructs displayed a bilayer. In some 2X and 3X constructs, rosette-like structures were detected by H&E staining under bright field (black arrows) and polarized light (white arrows). Mineralized tissue formation was indicated by H&E and confirmed by microCT. R: Rosette constructs. M: Mineralized constructs. MR: Mineralized Rosette constructs. Scale bars: 200 μm, inset 50 μm.

At 2W, 60% of *in vivo* implanted 1D-7D constructs were non-mineralized, non-rosette containing, 30% were non-mineralized rosette containing, and 10% contained rosette-like structures and mineralized tissue (Table 3.1). In contrast, 75% of 7D-7D constructs were non-mineralized rosette containing, and the remaining 25% were non-mineralized, non-rosette containing (Table 3.1). These results showed that 7D vs 1D culture in normal media facilitated DE cell rosette formation, even after *in vivo* growth.

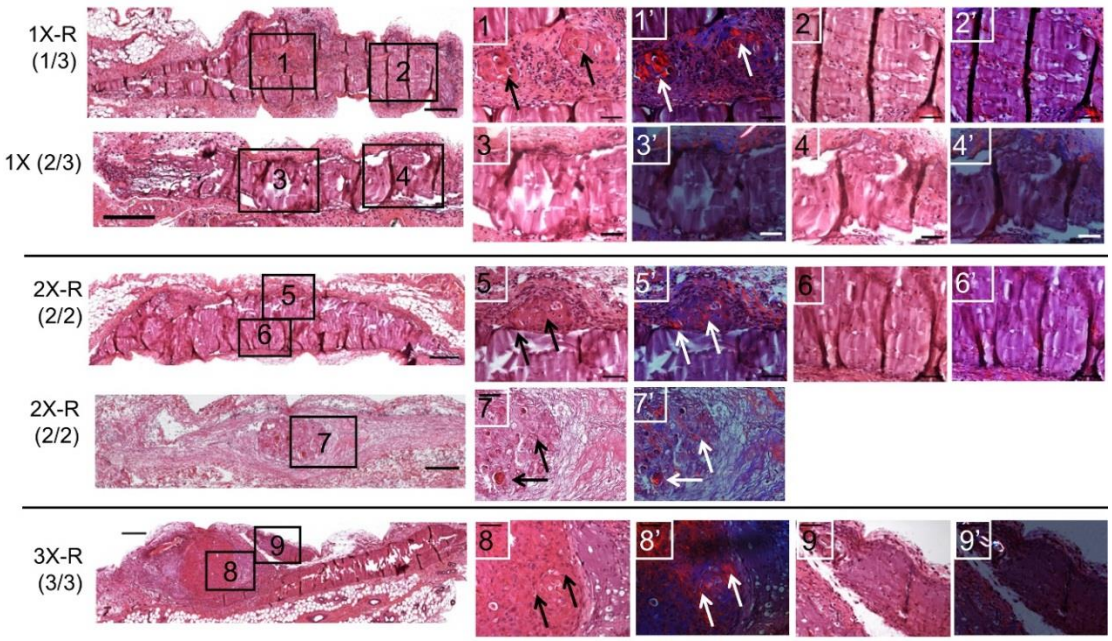

Figure 3.5. The Majority of 2W Bilayered 7D-7D *In Vivo* Constructs Contained Rosette-like Structures and Mineralized Tissue Matrix. All 2W, 2X and 3X 7D-7D constructs contained large rosette-like structures, detected by H&E staining under bright field (black arrows) and polarized light (white arrows). Only one 2W, 1X 7D-7D construct contained rosettes. No mineralized tissue formation was detected in 2W 7D-7D constructs. R: Rosette constructs. Scale bars: 200 µm, inset 50 µm.

At 4W, increased mineralized tissue formation and fewer rosettes were present in both 1D-7D and 7D-7D constructs (Figures 3.6 and 3.7). Only 10% of 4W, 1D-7D constructs were non-mineralized rosette containing (as compared to 30% at 2W), and 30% were mineralized non-rosette containing. The only mineralized rosette-containing construct (10%) was a 1D-7D 3X (similar to the 2W group). The remaining 1D-7D constructs (50%) were non-mineralized, non-rosette containing. Together, these results suggest that 2W non-mineralized rosette containing tissues gave rise to 4W mineralized or non-mineralized non-rosette, containing tissue.

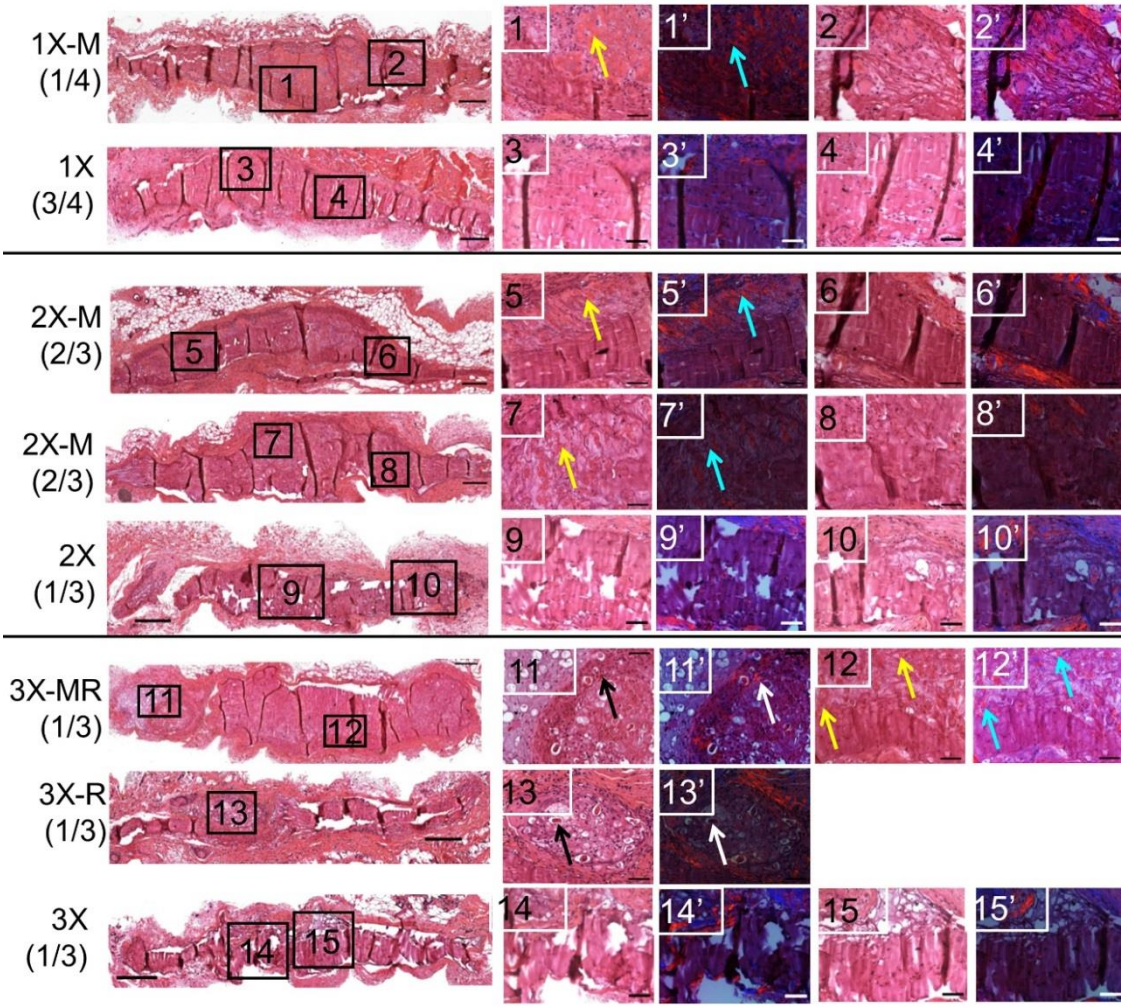

Figure 3.6. 4W, 1D-7D *In Vivo* Constructs Exhibited Rosette-like Structures and Mineralized Tissue Matrix. Mineralized tissue matrix was detected in all 4W 1D-7D constructs using H&E staining under bright field (yellow arrows) and polarized light (blue arrows). Rosette-like structures were observed only in 3X, constructs (white arrows). R: Rosette constructs. M: Mineralized constructs. MR: Mineralized Rosette constructs. Scale bars: 200 µm, inset 50 µm.

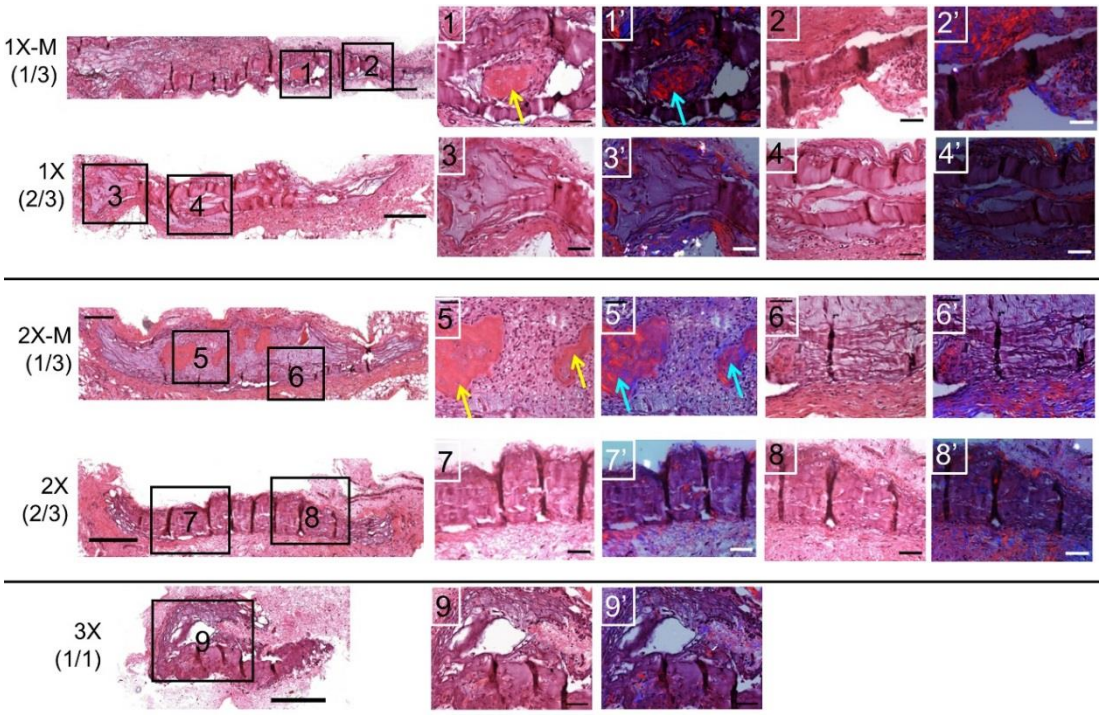

Figure 3.7. Mineralized Tissue Formation in 4W, 7D-7D *In Vivo* Constructs. H&E staining revealed mineralized tissue formation with bright field (yellow arrows) and polarized light (blue arrows) in 1X and 2X constructs. Rosette formation was not detected. M: Mineralized constructs. Scale bars: 200 µm, inset 50 µm.

3.3.4 Neovasculature localized to DE rosettes and mineralized tissues in *in vivo* constructs

After 2W *in vivo* implantation, all mineralized and rosette containing 1D-7D and 7D-7D constructs exhibited well-defined, ECAD positive rosettes surrounded by VM positive DM cells (Figure 3.8). The size of ECAD positive rosette-like structures generally increased with increased initial cell seeding density, and CD31 positive cells were present within and surrounding the rosettes (Figure 3.8). After 4W *in vivo* implantation, all rosette-containing 1D-7D constructs were ECAD positive (Figure 3.8), while mineralized non-rosette containing 4W 1D-7D constructs exhibited very few

ECAD positive cells (Figure 3.8), with VM and CD31 expression was detected within and surrounding mineralized tissue of 4W, 1D-7D mineralized non-rosette constructs. No rosettes were present in 4W 7D-7D constructs, although ECAD and CD31 were expressed in 4W 7D-7D 1X, and 2X mineralized non-rosette constructs (Figure 3.8). Robust VM expression was present within and around mineral tissues of the mineralized

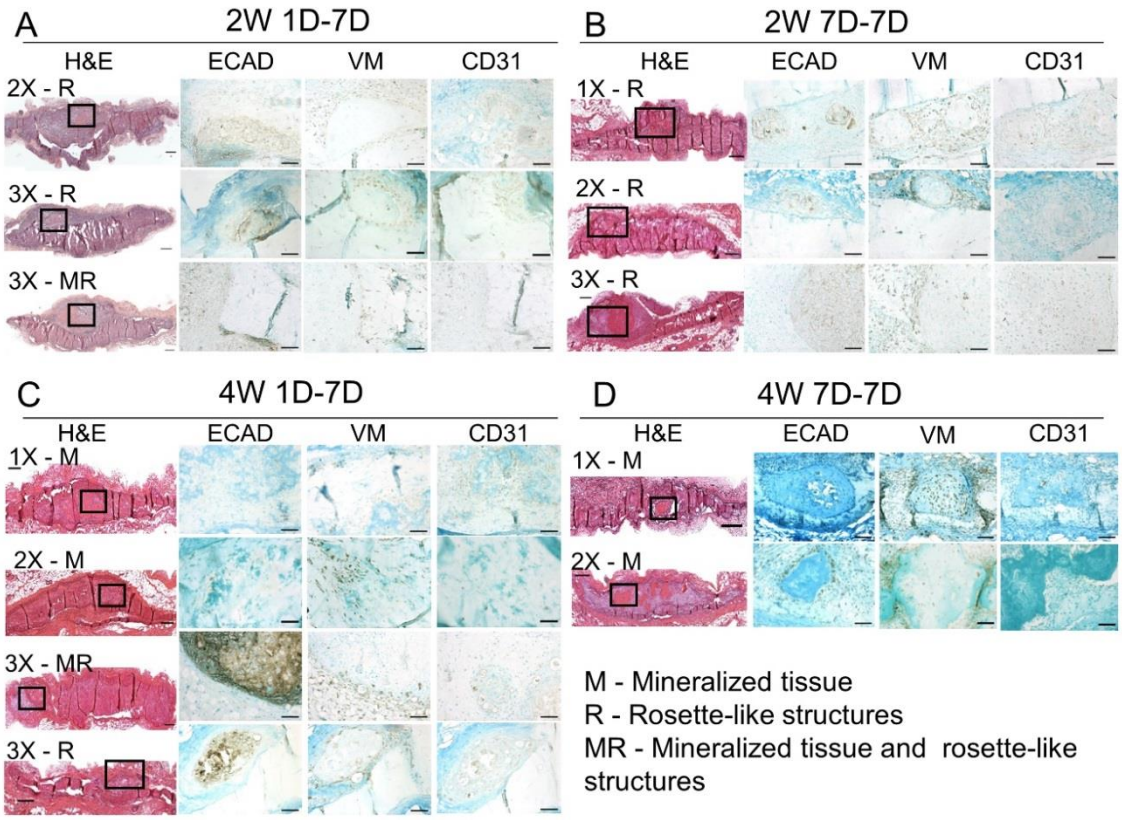

Figure 3.8. Neovasculature Localizes with DE Rosettes and Mineralized Tissues in *In Vivo* Constructs. ECAD positive DE cells formed rosette-like structures, which were surrounded by VM positive DM cells in 2W 1D-7D **(A)**, 2W 7D-7D **(B)**, and 4W 1D-7D **(C)** constructs. ECAD positive DE cells and or VM positive DM cells were also detected within and around mineralized tissues of 2W 1D-7D **(A)**, 4W 1D-7D **(C)**, and 4W 7D-7D **(D)**. CD31 expressing HUVECs colocalized to regions of DE rosette-like structures and mineralized tissue formation **(A-D)**. M: Mineralized tissue formation. R: Rosette formation. Scale Bar: H&E, 200 μm; ECAD/VM/CD31, 50 μm.

non-rosette 4W 7D-7D 1X, and 2X constructs (Figure 3.8).

Together, these results showed that CD31 positive neovasculature correlated with rosette and mineralized tissue formation in 2W and 4W 1D-7D and 7D-7D *in vivo* implanted constructs, and that 2W DE rosette structures induced 4W DM cell derived mineralized tissue formation.

3.3.5 Bioengineered tooth buds exhibited characteristic features of natural tooth buds

In natural tooth development, rosettes present in the DE stem cell (DESC) niche (*134, 135*) express the transcription factor Sox-2, which is important for DE stem cell maintenance, proliferation and competence (*135-138*). Remarkably, all of the DE rosettes in bioengineered tooth bud constructs exhibited robust Sox-2 expression at 2W (Figure 3.9 and Figure 3.10). Of these, the 2W, 2X and 3X constructs, also expressed another DESC niche marker, LEF-1 (*137, 139, 140*) (Figure 3.9), and the cell proliferation marker Ki67 (Figure 3.9). Together, these results suggested the formation of a bioengineered DESC niche. The bioengineered DESC niche was surrounded by condensing VM positive DM cells (Figure 3.9) that also expressed Fibroblast Growth Factor 3 (FGF3) (Figure 3.9), a known DM signaling molecule (*141, 142*). And basement membrane markers Collagen IV and Laminin (Figure 3.9). Bioengineered tooth buds expressed the DM ECM marker Fib2, and only weakly expressed the DE ECM cell marker Fib1, consistent with natural early tooth bud expression patterns (Figure 3.9) Strong expression of β-catenin and loss of ECAD within a cluster of DE cells within the

rosettes (Figure 3.9) indicate putative transit amplifying (TA) cells, which in natural tooth development migrate from the DESC niche to form enamel secreting ameloblasts (*143*). Importantly, a cluster of DE stem cell niche cells co-expressed FGF3 and Sonic

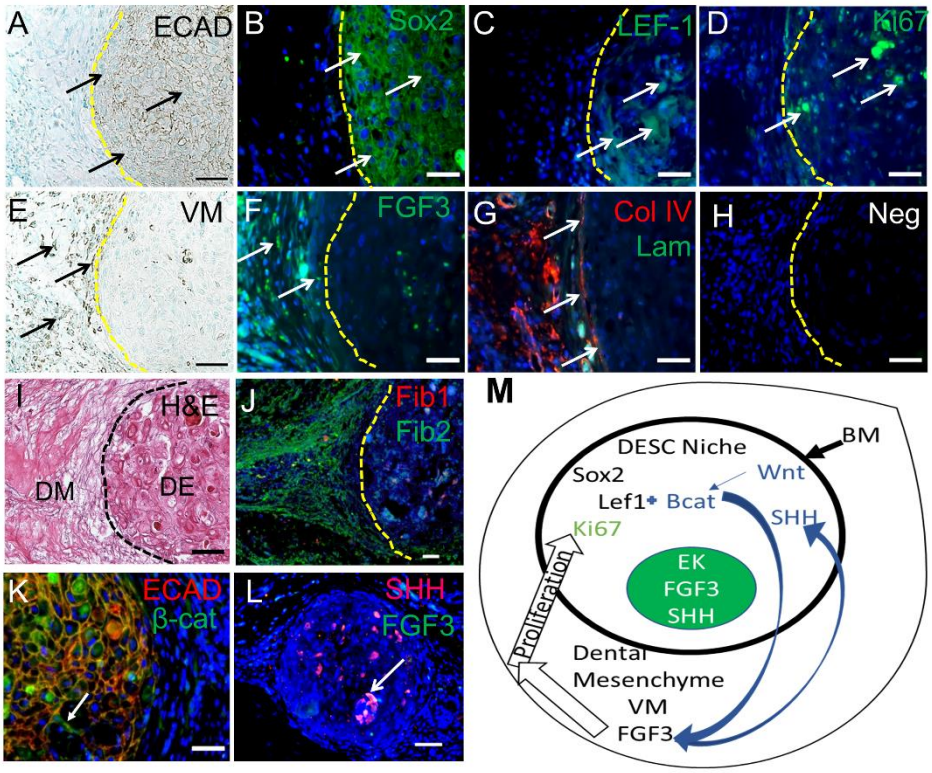

Figure 3.9. Bioengineered Tooth Buds Exhibit Characteristic Features of Natural Tooth Buds. All ECAD expressing rosette-like structures **(A)** strongly expressed Sox-2 **(B)**, LEF-1 **(C)**, and Ki67 **(D)**, suggesting the formation of a dental epithelial stem cell (DESC) niche. The putative DESC niche was surrounded by condensing DM cells that expressed vimentin (VM) **(E)** and Fibroblast Growth Factor 3 (FGF3) **(F)**, and was confined within a basement membrane that expressed Collagen IV (Col IV) and Laminin (Lam) **(G)**. Negative controls showed no fluorescent signal **(H)**. H&E staining revealed distinct DE and DM cell layers **(I)**, with fibrillin-1 (Fib1) expression was localized to the DE layer, and fibrillin-2 (Fib2) enriched in the DM layer **(J)**. Lack of (K) ECAD expression in Beta-Catenin (βcat) expressing cells suggest the presence of Transit-Amplifying (TA) cells. **(L)** A cluster of DE cells co-expressing Sonic Hedgehog (SHH) and FGF3 suggest the formation of a bioengineered enamel knot signaling center. **(M)** Schematic of early tooth bud markers expressed in bioengineered tooth bud including those of the DESC niche, enamel knot (EK), dental mesenchyme, and activated Wnt signaling **(M)**. Scale Bar: 50 μm.

Hedgehog (SHH), suggesting the formation of an enamel knot (EK) (Figure 3.9), a signaling center that directs natural tooth cusp formation (*144*). Finally, DE-expressed β-catenin and SHH adjacent to DM-expressed FGF3, indicated activation of the canonical Wnt signaling pathway (*145-148*). Together, these results demonstrated that bioengineered GelMA tooth bud constructs exhibited many important hallmark features of natural tooth development (Figure 3.9).

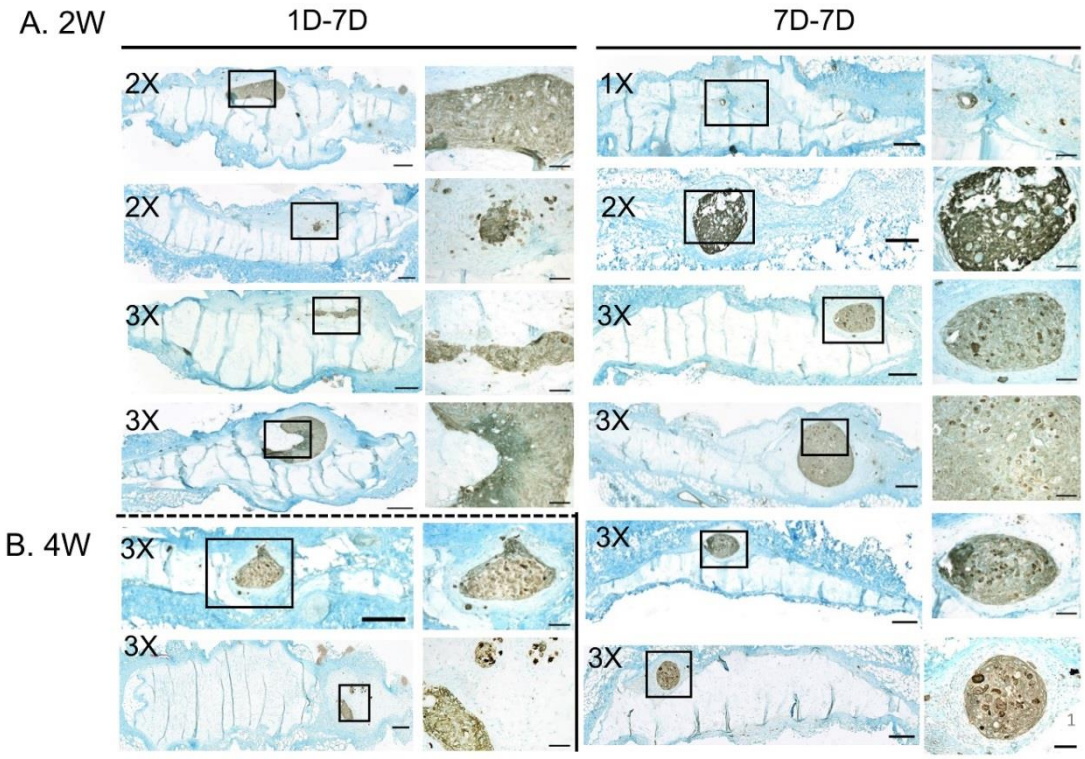

Figure 3.10. Robust Sox-2 Expressing Rosette-like Structures Indicate Putative DE Stem Cell (DESC) Niche in 2W and 4W *In Vivo* Implanted Constructs. IHC analysis revealed that all rosette containing 2W **(A)** and 4W **(B)** constructs expressed Sox-2, a marker of the DESC niche. Scale bars: 200 μm, inset 50 μm.

3.3.6 *In vivo* mineralized tissue formation increased with initial cell seeding density

Mineralized tissue that roughly adopted the size and shape of the construct was detected in 7/35 constructs (Figure 3.11). Highest mineral density was located in the center surrounded by intermediate, and then lowest mineral density at the periphery (Figure 3.11, and Videos 1 and 2). The highest maximum and average mineral densities and volumes were identified in 2X 1D-7D and 7D-7D constructs (Figure 3.11), which at 4W exhibited the highest mineralized tissue formation.

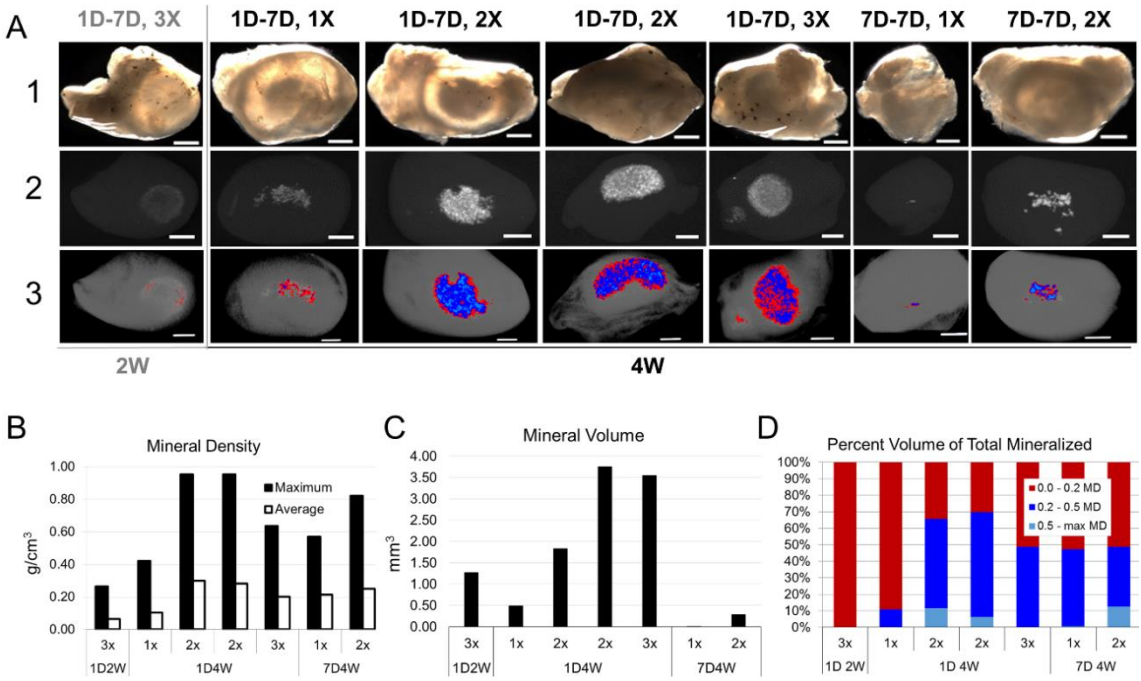

Figure 3.11. Mineralized Tissue Formation in *In Vivo* Implanted Tooth Bud Constructs. Bright field **(A1)** and Micro-CT **(A2)** images of *in vivo* constructs. Maximum and average mineral densities values correlated with initial cell seeding densities **(B)**. 2X, 1D-7D and 2X, 7D-7D constructs exhibited highest mineralized tissue density. Initial cell seeding density correlated with mineralized tissue volume **(C)**. 2X, 1D-7D and 2X, 7D-7D constructs also exhibited the greatest volume of highest mineral density **(D)**. Low density mineralized tissue was located around the periphery, while intermediate and high density mineralized tissues were located in the center **(A3)**. Scale bar: 200 µm.

3.3.7 Ameloblast, odontoblast and osteoblast differentiation in *in vivo* implanted constructs

At 2W, robust AM and DSPP expression was detected within mineralized tissue and rosette containing 2X and 3X 1D-7D constructs (Figure 3.12), and in all 2W 7D-7D constructs (Figure 3.12). No OC expression was detected in 2W 2X 1D-7D (Figure 3.12) or 2W 1X 7D-7D constructs (Figure 3.12), and only weak, punctate OC expression was detected in 2W 3X 1D-7D (Figure 3.12) and 2W 2X and 3X 7D-7D constructs (Figure 3.12). Interesting expression patterns were revealed in 4W constructs (Figure 3.12), where in 1D-7D constructs, all but 2X exhibited strong AM expression, DSPP was only expressed in the 1X, and OC was expressed in 2X and 3X. At 4Ws, all 7D-7D constructs expressed AM, with DSPP and weak OC only in 2X. These results showed that 1D-7D conditions were more conducive to OC expressing bone differentiation, while 7D-7D promoted odontogenic tissue differentiation. Furthermore, 2X constructs exhibited the highest mineral density, and odontoblast and ameloblast differentiation.

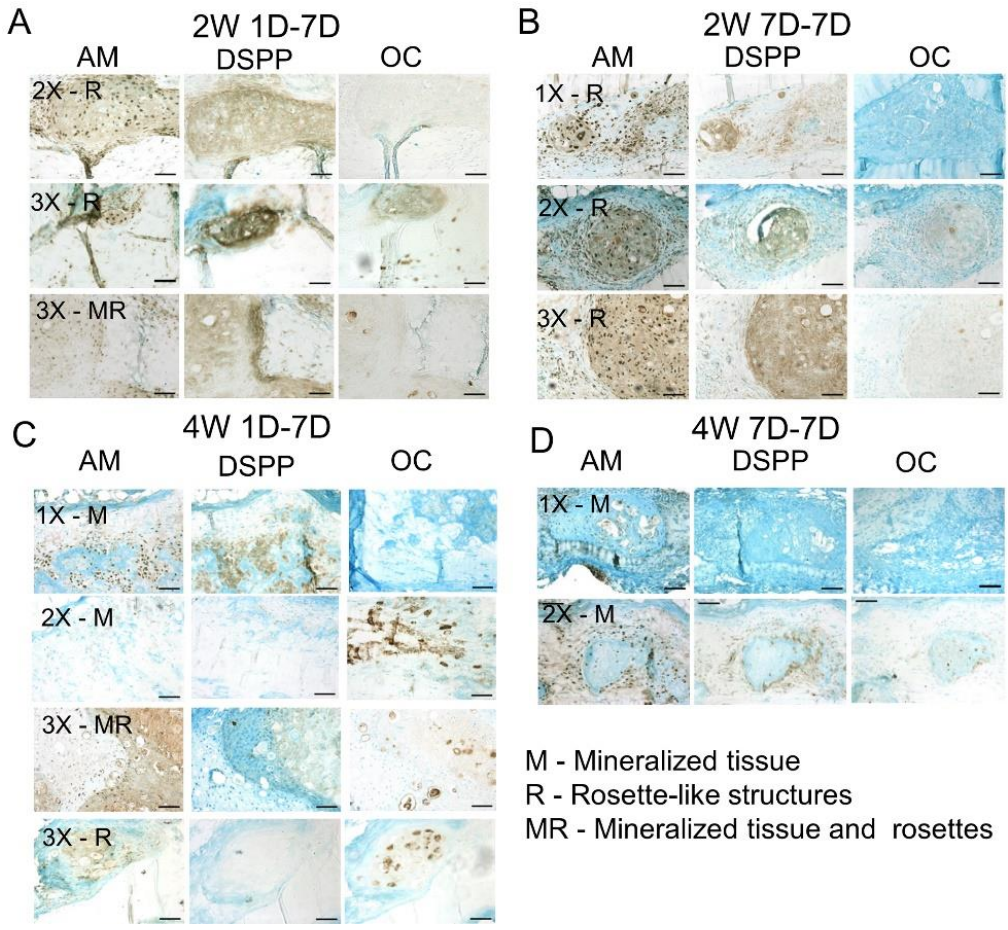

Figure 3.12. Ameloblast, Odontoblast and Osteoblast Differentiation in *In Vivo* Implanted Tooth Bud Constructs. AM and DSPP expression was localized to organized rosette-like structures, and around and within mineralized tissues in 2W 1D-7D **(A)**, 2W 7D-7D **(B)**, and 4W 1D-7D **(C)** constructs. In contrast, 4W 1D-7D 2X mineralized constructs lacked AM and DSPP expression **(C)**, the 4W 1D-7D 2X mineralized rosette containing construct lacked DSPP expression **(C)**, and the 4W 7D-7D 1X mineralized construct lacked DSPP expression **(D)**. Weak OC expression was detected in rosette-like structures, and strong punctate OC expression was localized to mineralized tissues of 2W 1D-7D **(A)**, 2W 7D-7D **(B)**, 4W 1D-7D **(C)**, and 4W 7D-7D constructs. OC was not detected in the 2W 1D-7D 2X, or the 2W 7D-7D 1X rosette-containing constructs **(A, B)**, or the 4W 7D-7D 1X mineralized construct **(D)**. M: Mineralized tissue formation. R: Rosette-like formation. Scale Bar: 50 µm.

3.4 Discussion

The purpose of this study was to improve our bioengineered tooth bud model by comparing: 1) sequential versus simultaneous photo-crosslinking of GelMA encapsulated DE and DM cell layers; 2) initial cell seeding density with that of *in vivo* implanted constructs; and 3) 1D-7D versus 7D-7D *in vitro* culture conditions prior to implantation.

Our analyses showed that: 1) sequential photo-crosslinking resulted in the formation of distinct DE and DM layers in all conditions, in both *in vitro* cultured and *in vivo* implanted constructs; 2) HUVEC-derived neovascular-like structures formed in all conditions; 3) bioengineered tooth buds exhibited many features characteristic of natural tooth buds, including the DESC niche, EK signaling center, and TA cells and activated conical WNT signaling; and 4) bioengineered tooth buds implanted in vivo exhibited dental cell differentiation marker expression and mineralized dental tissue formation.

With respect to *in vitro* culture conditions, while 1D-7D *in vitro* cultured constructs generally exhibited higher cell viability prior to implantation, 7D-7D cultured constructs formed more rosette-like structures.

With respect to mineralized tissue formation, the 4W 2X cell seeding density exhibited the greatest mineralized tissue volume and density, consistent with reports on the influence of cell seeding density on mesenchymal cell fate (*127, 149, 150*). *In vivo* implanted 7D-7D constructs more consistently supported dental cell differentiation as compared to 1D-7D constructs, which more commonly supported osteoblast differentiation. Most cells either expressed either DSPP, OC, or AM, with only a small number expressing both DSPP and OC, or DSPP and AM (Figure 3.13). Although 2X

1D-7D mineral volume was higher than 7D-7D, mineral density was similar in 1D-7D and 7D-7D constructs. Importantly, 7D-7D constructs formed DSPP expressing mineralized tissues, while 1D-7D constructs formed OC expressing bone tissue.

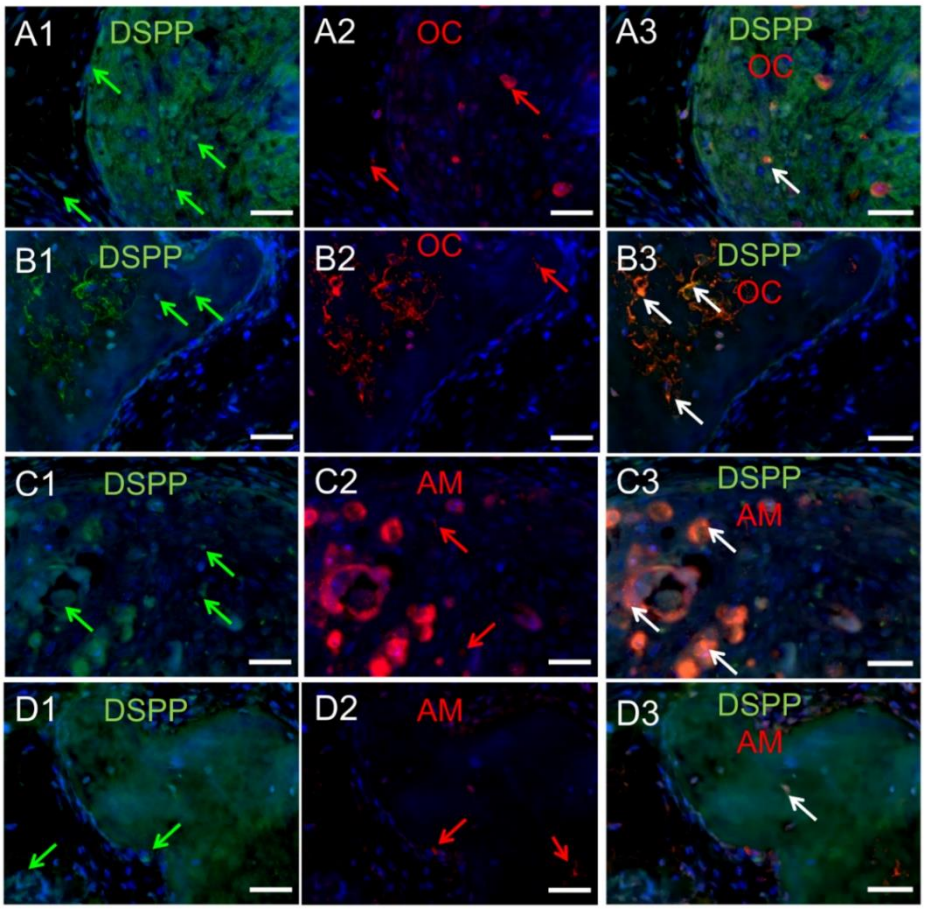

Figure 3.13. Investigating Dental Cell Differentiation Marker Co-localization. Representative IF images demonstrate that the majority of cells within the rosettes **(A1, A2)** and in mineralized tissue matrix **(B2, B2)** expressed either DSPP (green arrows) or OC (red arrows), and a few expressed both **(A3, B3)**. Additionally, both OC and DSPP co-localized to the mineralized tissue matrix **(B3)**. Similarly, representative IF images demonstrate that individual cells within rosette containing constructs **(C1, C2)** and in mineralized tissues **(D1, D2)** expressed DSPP (green arrows) or AM (red arrows), while DSPP was predominantly expressed in the mineralized tissue matrix **(D3)**. Co-expression of DSPP and AM was also evident **(C3, D3)**. Scale Bar: 200 μm (A-D), 50 μm (A'-D').

A key factor for bioengineered mineralized tissue formation was the formation of CD31 positive HUVEC derived neovasculature. Neovasculature was present in 2W and 4W rosette-like structures, and in mineralized tissues in both 1D-7D and 7D-7D constructs, consistent with natural tooth development (*91, 93*) and bioengineered tooth development (*79, 126*) (*151*).

Importantly, bioengineered tooth buds exhibited features of the natural DE stem cell niche. Including robust Sox2 expression. Sox-2 positive DE cells were also present in *in vitro* 1D-7D and 7D-7D constructs prior to *in vivo* implantation (Figure 3.14). In natural tooth development, Sox-2 and Lef-1 cooperate with Pitx2 to regulate DE stem cell maintenance, development and self-renewal (*137, 139, 152*). Interestingly, bioengineered

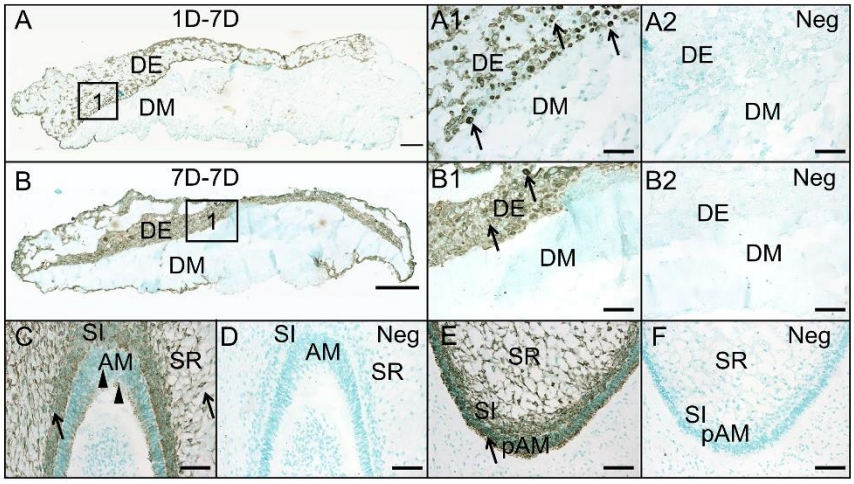

Figure 3.14. Sox-2 expressing DE stem cell niche in *in vitro* cultured tooth bud constructs. IHC analysis identified Sox-2 positive cells located in the DE layer of 1D-7D **(A, A1)** and 7D-7D **(B, B1)** *in vitro* cultured constructs. Negative controls exhibited no positive staining **(A2, B2, F)**. Sox-2 expression in *in* vitro cultured constructs resembled Sox-2 expression in the stratum intermedium (SI) and stellate reticulum (SR) DE layers of the natural pig tooth bud **(C, arrows)**. Differentiated mature ameloblasts (AM) located at the natural tooth bud cusp lose Sox-2 expression as they differentiate **(C, arrowheads)**. Immature Pre-ameloblasts located in the trough between two cusps exhibit robust Sox-2 expression **(E, arrow)**. Scale bars: 200 µm (A, B, C, D), 50 µm (A1, A2, B1, B2, E, F).

tooth buds also expressed dental cell specific ECM markers Fib1 and Fib2, which in natural teeth are expressed in later stage DE, and early stage DM (*153*).

Our analyses suggest that bioengineered DE rosettes gave rise to mineralized tissue formation as is observed in natural teeth, where Sox-2 positive cells leave the cervical loop to become TA cells that terminally differentiate into ameloblasts (*154, 155*). Activated Wnt signaling was demonstrated by SHH and β-catenin expression in DE rosettes, and FGF3 in adjacent DM. Co-expression of SHH and FGF3 in tightly packed clusters of DE cells identified putative EK signaling centers.

Although these results demonstrate substantial improvements to our previous bioengineered tooth model, certain limitations still exist. We observed variability within sample groups, perhaps caused by the time required to spot curing individual samples. In the future, we hope to devise methods to spot cure samples all at once. In addition, we found no evidence of DE or DM cell polarization, or distinct dentin and enamel crystal structures, all classic features of natural teeth. These results suggest the lack of sufficient cues within the GelMA constructs as they are currently made.

Despite these limitations, here we have validated improved methods to bioengineer highly sophisticated tooth buds. This is the first to report the formation of bioengineered tooth buds, created from post-natal dental cells that recapitulate many unique features of natural tooth development, including the DESC niche, TA cells, EK signaling center, and activated Wnt signaling. We propose this model as an important step forward towards eventual clinical applications in regenerative dentistry.

Chapter 4: Discussion

Current clinical applications are highly focused on the use of inert artificial materials to repair dental defects. The gold standard for tooth replacement therapy is dental implantation of a prosthetic, usually composed of a titanium root and artificial crown. These implants have proven to be successful; however there are complications that can arise. The field of Regenerative Dentistry aims to overcome such limitations by providing biologically-based alternatives that more accurately resemble the natural dental tissue.

The work presented here describes a tooth bud model that can be used as a future platform for whole tooth bioengineering in humans. Since most dental tissues form at a very early developmental stage, natural tooth development was used as a guide to bioengineer the tooth bud model. Natural tooth development is regulated by the continual and reciprocal signaling events and interactions between the DE and DM tissues layers. The tooth bud model was created to mimic the natural early bilayer organization which would promote differentiation and mineralized tissue formation at the bilayer interface, such as in natural tooth development. For future clinical applications, autologous dental cells would be isolated from the patient, encapsulated within GelMA hydrogel to form a bioengineered tooth bud, and then implanted at the site of tooth loss where it is expected to further develop, erupt and function just as well as a natural tooth. This report describes the characterization and optimization of the current GelMA tooth bud model.

The tooth bud model is fabricated by encapsulating post-natal porcine dental epithelial and dental mesenchymal cells along with HUVECs within GelMA hydrogel. The hypothesis stated that GelMA hydrogels can be used as a supportive scaffold for the

formation of 3D biomimetic tooth buds of predetermined size and shape. The preliminary work described in Chapter 2 validates GelMA hydrogel as a supportive scaffold for appropriate mechanical tunability, viable cell activity, and differentiation of encapsulated dental cells. Select GelMA formulas were shown to resemble the mechanical properties of natural dental tissues, allow cell attachment, and support increased MMP activity as well as metabolic activity. Furthermore, this was the first report to demonstrate organized formation of dental mesenchymal cells surrounding endothelial cells to create an *in vitro* vascular network. In this way, DM cells were likely to behave as pericyte-like cells.

When implanted subcutaneously, mineralized tissue formed and adopted the size and shape of the GelMA construct, which suggests that the size and shape of a bioengineered tooth can be predetermined. DE-derived expression of Amelogenin and robust DM-derived expression of DSPP and OC indicate dental cell differentiation of DE cells into ameloblast-like cells and DM cells into osteodentin producing odontoblasts. In addition, HUVECs lined capillary networks contributed to the innervation and formation of functional neovasculature. This preliminary study was important as it showed that GelMA hydrogel had the potential to serve as a scaffold material for a tooth bud model.

Chapter 3 describes the optimization study which focused to improve the preliminary model and address limitations such as cell layer mixing. Sequential photocrosslinking of each dental cell layer resulted in defined layers that were maintained through *in vitro* culture and *in vivo* growth, which led to increased DE and DM specific tissue formation. Interestingly, this potentially resulted in the recapitulation of several events that occur during tooth development. Most importantly, the DESC niche was

identified within the DE layer of the bioengineered tooth bud. This is a significant finding as it is the first to demonstrate that postnatal dental cells can be used to create a stem cell niche. This study also describes the presence of a basement membrane, condensing DM cells, TA cells, active EK signaling center, canonical Wnt signaling, and fibrillin expression that resembles that of naturally developing tooth buds. Furthermore, the results suggest that extended time in culture lead to increased formation of DE rosette-like structures. The results also indicate that increased cell seeding density resulted in increased mineralized tissue formation that resembled dentin nodular formation. All the of the results presented in chapter 2 and chapter 3support the GelMA tooth bud model as a promising step towards the future in regenerative dentistry.

The limitations of the GelMA tooth bud model include lack of dentin and enamel formation. Although enamel and dentin were not identified in this model, the essential proteins found in dentin and enamel were present. Furthermore, the model exhibited many aspects that are present prior to dentin and enamel formation. The goal for future experimental work is to provide the tooth bud model with an environment that harbors intrinsic factors that will aid in distinct enamel and dentin formation.

The overall results presented here are significant in that they define new methods to create bioengineered tooth buds that closely resemble naturally formed tooth buds, both morphologically and at the molecular level. It is also significant that these bioengineered tooth buds were created from clinically relevant post-natal cell populations, and not from embryonic tooth cells or tissues. This is the first report to demonstrate the recapitulation of hallmark features of natural tooth development in a

post-natal cell derived bioengineered tooth bud model. In conclusion, the results presented from these studies suggest that the GelMA tooth bud model can potentially advance the current field of regenerative dentistry by providing a platform for whole tooth replacement therapies.

Chapter 5: Bibliography

1. T. Vos, A. D. Flaxman, M. Naghavi, R. Lozano, C. Michaud, M. Ezzati, K. Shibuya, J. A. Salomon, e. al., Years lived with disability (YLDs) for 1160 sequelae of 289 diseases and injuries 1990–2010: a systematic analysis for the Global Burden of Disease Study 2010. *The Lancet* **380**, 2163-2196 (2012).
2. G. Greenstein, J. Cavallaro, G. Romanos, D. Tarnow, Clinical Recommendations for Avoiding and Managing Surgical Complications Associated With Implant Dentistry: A Review. *Journal of Periodontology* **79**, 1317-1329 (2008).
3. R. E. Jung, B. E. Pjetursson, R. Glauser, A. Zembic, M. Zwahlen, N. P. Lang, A systematic review of the 5-year survival and complication rates of implant-supported single crowns. *Clin. Oral Implants Res.* **19**, 119-130 (2008).
4. A. H. Yen, P. C. Yelick, Dental Tissue Regeneration – A Mini-Review. *Gerontology* **57**, 85-94 (2011).
5. W.-F. Lai, J.-M. Lee, H.-S. Jung, Molecular and engineering approaches to regenerate and repair teeth in mammals. *Cell. Mol. Life Sci.* **71**, 1691-1701 (2014).
6. I. Thesleff, Epithelial-mesenchymal signalling regulating tooth morphogenesis. *Journal of Cell Science* **116**, 1647-1648 (2003).
7. I. Thesleff, P. Nieminen, Tooth morphogenesis and cell differentiation. *Curr. Opin. Cell Biol.* **8**, 844-850 (1996).
8. Y. D. Zhang, Z. Chen, Y. Q. Song, C. Liu, Y. P. Chen, Making a tooth: growth factors, transcription factors, and stem cells. *Cell Res.* **15**, 301-316 (2005).
9. I. Thesleff, P. Sharpe, Signalling networks regulating dental development. *Mech. Dev.* **67**, 111-123 (1997).
10. I. Thesleff, The genetic basis of tooth development and dental defects. *Am. J. Med. Genet. A* **140A**, 2530-2535 (2006).
11. J. V. Ruch, H. Lesot, V. Karcher-Djuricic, J. M. Meyer, M. Olive, Facts and Hypotheses Concerning the Control of Odontoblast Differentiation. *Differentiation* **21**, 7-12 (1982).
12. M. Jussila, I. Thesleff, Signaling Networks Regulating Tooth Organogenesis and Regeneration, and the Specification of Dental Mesenchymal and Epithelial Cell Lineages. *Cold Spring Harb. Perspect. Biol.* **4**, (2012).
13. I. Thesleff, S. Vainio, M. Jalkanen, Cell-matrix interactions in tooth development. *The International Journal of Developmental Biology* **33**, 91-97 (1989).
14. A. Tucker, P. Sharpe, The cutting-edge of mammalian development; how the embryo makes teeth. *Nat. Rev. Genet.* **5**, 499-508 (2004).
15. S. Glasstone, The development of tooth germs on the chick chorio-allantois. *J. Anat.* **88**, 392-399 (1954).
16. M. Mina, E. J. Kollar, The induction of odontogenesis in non-dental mesenchyme combined with early murine mandibular arch epithelium. *Arch. Oral Biol.* **32**, 123-127 (1987).
17. M. T. Duailibi, S. E. Duailibi, C. S. Young, J. D. Bartlett, J. P. Vacanti, P. C. Yelick, Bioengineered Teeth from Cultured Rat Tooth Bud Cells. *J. Dent. Res.* **83**, 523-528 (2004).

18. C. S. Young, H. Abukawa, R. Asrican, M. Ravens, M. J. Troulis, L. B. Kaban, J. P. Vacanti, P. C. Yelick, Tissue-engineered hybrid tooth and bone. *Tissue Eng.* **11**, (2005).
19. S. E. Duailibi, M. T. Duailibi, W. Zhang, R. Asrican, J. P. Vacanti, P. C. Yelick, Bioengineered Dental Tissues Grown in the Rat Jaw. *J. Dent. Res.* **87**, 745-750 (2008).
20. Z. H. Gao, L. Hu, G. L. Liu, F. L. Wei, Y. Liu, Z. H. Liu, Z. P. Fan, C. M. Zhang, J. S. Wang, S. L. Wang, Bio-Root and Implant-Based Restoration as a Tooth Replacement Alternative. *Journal of Dental Research*, (2016).
21. K.-C. Yang, Y. Kitamura, C.-C. Wu, H.-H. Chang, T.-Y. Ling, T.-F. Kuo, Tooth Germ-Like Construct Transplantation for Whole-Tooth Regeneration: An In Vivo Study in the Miniature Pig. *Artif. Organs* **40**, E39-E50 (2016).
22. M. Bhoj, C. Zhang, D. W. Green, A First Step in De Novo Synthesis of a Living Pulp Tissue Replacement Using Dental Pulp MSCs and Tissue Growth Factors, Encapsulated within a Bioinspired Alginate Hydrogel. *J. Endod.* **41**, 1100-1107 (2015).
23. S. Gronthos, M. Mankani, J. Brahim, P. G. Robey, S. Shi, Postnatal human dental pulp stem cells (DPSCs) in vitro and in vivo. *Proc. Natl. Acad. Sci. U. S. A.* **97**, 13625-13630 (2000).
24. M. Miura, S. Gronthos, M. Zhao, B. Lu, L. W. Fisher, P. G. Robey, S. Shi, SHED: Stem cells from human exfoliated deciduous teeth. *Proc. Natl. Acad. Sci. U. S. A.* **100**, 5807-5812 (2003).
25. M. M. Cordeiro, Z. Dong, T. Kaneko, Z. Zhang, M. Miyazawa, S. Shi, A. J. Smith, J. E. Nör, Dental Pulp Tissue Engineering with Stem Cells from Exfoliated Deciduous Teeth. *J. Endod.* **34**, 962-969 (2008).
26. C. M. Sedgley, T. M. Botero, Dental Stem Cells and Their Sources. *Dent. Clin. North Am.* **56**, 549-561 (2012).
27. W. Sonoyama, Y. Liu, D. Fang, T. Yamaza, B.-M. Seo, C. Zhang, H. Liu, S. Gronthos, C.-Y. Wang, S. Shi, S. Wang, Mesenchymal Stem Cell-Mediated Functional Tooth Regeneration in Swine. *PLoS One* **1**, e79 (2006).
28. C. Morsczeck, W. Götz, J. Schierholz, F. Zeilhofer, U. Kühn, C. Möhl, C. Sippel, K. H. Hoffmann, Isolation of precursor cells (PCs) from human dental follicle of wisdom teeth. *Matrix Biol.* **24**, 155-165 (2005).
29. W. Guo, Y. He, X. Zhang, W. Lu, C. Wang, H. Yu, Y. Liu, Y. Li, Y. Zhou, J. Zhou, M. Zhang, Z. Deng, Y. Jin, The use of dentin matrix scaffold and dental follicle cells for dentin regeneration. *Biomaterials* **30**, 6708-6723 (2009).
30. B.-M. Seo, M. Miura, S. Gronthos, P. Mark Bartold, S. Batouli, J. Brahim, M. Young, P. Gehron Robey, C. Y. Wang, S. Shi, Investigation of multipotent postnatal stem cells from human periodontal ligament. *The Lancet* **364**, 149-155.
31. Y. Shinmura, S. Tsuchiya, K.-i. Hata, M. J. Honda, Quiescent epithelial cell rests of Malassez can differentiate into ameloblast-like cells. *J. Cell. Physiol.* **217**, 728-738 (2008).
32. M. J. Honda, Y. Shinohara, K. I. Hata, M. Ueda, Subcultured Odontogenic Epithelial Cells in Combination With Dental Mesenchymal Cells Produce

Enamel–Dentin-Like Complex Structures. *Cell Transplant.* **16**, 833-847 (2007).
33. Y. Liu, M. Jiang, W. Hao, W. Liu, L. Tang, H. Liu, Y. Jin, Skin epithelial cells as possible substitutes for ameloblasts during tooth regeneration. *J. Tissue Eng. Regen. Med.* **7**, 934-943 (2013).
34. A. Angelova Volponi, M. Kawasaki, P. T. Sharpe, Adult Human Gingival Epithelial Cells as a Source for Whole-tooth Bioengineering. *J. Dent. Res.*, (2013).
35. K. Takahashi, S. Yamanaka, Induction of Pluripotent Stem Cells from Mouse Embryonic and Adult Fibroblast Cultures by Defined Factors. *Cell* **126**, 663-676 (2006).
36. P. Karagiannis, K. Eto, Ten years of induced pluripotency: from basic mechanisms to therapeutic applications. *Development* **143**, 2039-2043 (2016).
37. P. Liu, Y. Zhang, S. Chen, J. Cai, D. Pei, Application of iPS Cells in Dental Bioengineering and Beyond. *Stem Cell Reviews and Reports* **10**, 663-670 (2014).
38. H. Egusa, K. Okita, H. Kayashima, G. Yu, S. Fukuyasu, M. Saeki, T. Matsumoto, S. Yamanaka, H. Yatani, Gingival Fibroblasts as a Promising Source of Induced Pluripotent Stem Cells. *PLoS One* **5**, e12743 (2010).
39. N. Wada, B. Wang, N. H. Lin, A. L. Laslett, S. Gronthos, P. M. Bartold, Induced pluripotent stem cell lines derived from human gingival fibroblasts and periodontal ligament fibroblasts. *J. Periodontal Res.* **46**, 438-447 (2011).
40. X. Yan, H. Qin, C. Qu, R. S. Tuan, S. Shi, G. T. J. Huang, iPS Cells Reprogrammed From Human Mesenchymal-Like Stem/Progenitor Cells of Dental Tissue Origin. *Stem Cells Dev.* **19**, 469-480 (2009).
41. L. Liu, Y.-F. Liu, J. Zhang, Y.-Z. Duan, Y. Jin, Ameloblasts serum-free conditioned medium: bone morphogenic protein 4-induced odontogenic differentiation of mouse induced pluripotent stem cells. *J. Tissue Eng. Regen. Med.* **10**, 466-474 (2016).
42. N. Ozeki, M. Mogi, R. Kawai, H. Yamaguchi, T. Hiyama, K. Nakata, H. Nakamura, Mouse-Induced Pluripotent Stem Cells Differentiate into Odontoblast-Like Cells with Induction of Altered Adhesive and Migratory Phenotype of Integrin. *PLoS One* **8**, e80026 (2013).
43. S. Kuchler-Bopp, T. Bécavin, T. Kökten, J. L. Weickert, L. Keller, H. Lesot, E. Deveaux, N. Benkirane-Jessel, Three-dimensional Micro-culture System for Tooth Tissue Engineering. *J. Dent. Res.* **95**, 657-664 (2016).
44. W. Zhang, B. Vázquez, P. C. Yelick, Bioengineered post-natal recombinant tooth bud models. *J. Tissue Eng. Regen. Med.*, n/a-n/a (2014).
45. A. J. Engler, S. Sen, H. L. Sweeney, D. E. Discher, Matrix Elasticity Directs Stem Cell Lineage Specification. *Cell* **126**, 677-689 (2006).
46. K. M. Galler, R. N. D'Souza, J. D. Hartgerink, Biomaterials and their potential applications for dental tissue engineering. *J. Mater. Chem.* **20**, 8730-8746 (2010).
47. M. Oshima, T. Tsuji, in *Engineering Mineralized and Load Bearing Tissues*, E. L. Bertassoni, G. P. Coelho, Eds. (Springer International Publishing, Cham, 2015), pp. 255-269.

48. N. Monteiro, P. C. Yelick, Advances and perspectives in tooth tissue engineering. *J. Tissue Eng. Regen. Med.*, n/a-n/a (2016).
49. C. S. Young, S. Terada, J. P. Vacanti, M. Honda, J. D. Bartlett, P. C. Yelick, Tissue Engineering of Complex Tooth Structures on Biodegradable Polymer Scaffolds. *J. Dent. Res.* **81**, 695-700 (2002).
50. H. Abukawa, W. Zhang, C. S. Young, R. Asrican, J. P. Vacanti, L. B. Kaban, M. J. Troulis, P. C. Yelick, Reconstructing Mandibular Defects Using Autologous Tissue-Engineered Tooth and Bone Constructs. *J. Oral Maxillofac. Surg.* **67**, 335-347 (2009).
51. W. Zhang, H. Abukawa, M. J. Troulis, L. B. Kaban, J. P. Vacanti, P. C. Yelick, Tissue engineered hybrid tooth–bone constructs. *Methods* **47**, 122-128 (2009).
52. R. S. Prescott, R. Alsanea, M. I. Fayad, B. R. Johnson, C. S. Wenckus, J. Hao, A. S. John, A. George, In Vivo Generation of Dental Pulp-like Tissue by Using Dental Pulp Stem Cells, a Collagen Scaffold, and Dentin Matrix Protein 1 after Subcutaneous Transplantation in Mice. *J. Endod.* **34**, 421-426 (2008).
53. W. Zhang, I. P. Ahluwalia, R. Literman, D. L. Kaplan, P. C. Yelick, Human dental pulp progenitor cell behavior on aqueous and hexafluoroisopropanol (HFIP) based silk scaffolds. *J. Biomed. Mater. Res. A* **97**, 414-422 (2011).
54. W.-P. Xu, W. Zhang, R. Asrican, H.-J. Kim, D. L. Kaplan, P. C. Yelick, Accurately Shaped Tooth Bud Cell–Derived Mineralized Tissue Formation on Silk Scaffolds. *Tissue Eng. Part A* **14**, 549-557 (2008).
55. C. Schubert, M. C. van Langeveld, L. A. Donoso, Innovations in 3D printing: a 3D overview from optics to organs. *Br. J. Ophthalmol.* **98**, 159-161 (2014).
56. C. L. Ventola, Medical Applications for 3D Printing: Current and Projected Uses. *Pharmacy and Therapeutics* **39**, 704-711 (2014).
57. X. Cui, T. Boland, D. D. D'Lima, M. K. Lotz, Thermal Inkjet Printing in Tissue Engineering and Regenerative Medicine. *Recent patents on drug delivery & formulation* **6**, 149-155 (2012).
58. I. T. Ozbolat, Y. Yu, Bioprinting Toward Organ Fabrication: Challenges and Future Trends. *IEEE Trans. Biomed. Eng.* **60**, 691-699 (2013).
59. C. Fuellhase, R. Soler, K. E. Andersson, A. Atala, J. J. Yoo, 264 GENERATION OF ORGANIZED BLADDER TISUE CONSTRUCTS USING A NOVEL HYBRID PRINTING SYSTEM. *European Urology Supplements* **8**, 186.
60. S. Bartlett, Printing organs on demand. *The Lancet Respiratory Medicine* **1**, 684 (2013).
61. Y. Chen, M. Bei, I. Woo, I. Satokata, R. Maas, Msx1 controls inductive signaling in mammalian tooth morphogenesis. *Development* **122**, 3035-3044 (1996).
62. R. N. D'Souza, R. P. Happonen, N. M. Ritter, W. T. Butler, Temporal and spatial patterns of transforming growth factor-β1 expression in developing rat molars. *Arch. Oral Biol.* **35**, 957-965 (1990).
63. I. Thesleff, M. Mikkola, in *Int. Rev. Cytol.* (Academic Press, 2002), vol. Volume 217, pp. 93-135.

64. S. Vainio, I. Karavanova, A. Jowett, I. Thesleff, Identification of BMP-4 as a signal mediating secondary induction between epithelial and mesenchymal tissues during early tooth development. *Cell* **75**, 45-58 (1993).
65. A. H. Jheon, K. Seidel, B. Biehs, O. D. Klein, From molecules to mastication: the development and evolution of teeth. *Wiley Interdisciplinary Reviews: Developmental Biology* **2**, 165-182 (2013).
66. J. Jernvall, T. Aberg, P. Kettunen, S. Keranen, I. Thesleff, The life history of an embryonic signaling center: BMP-4 induces p21 and is associated with apoptosis in the mouse tooth enamel knot. *Development* **125**, 161-169 (1998).
67. A. Vaahtokari, T. Åberg, J. Jernvall, S. Keränen, I. Thesleff, The enamel knot as a signaling center in the developing mouse tooth. *Mech. Dev.* **54**, 39-43 (1996).
68. X.-P. Wang, M. Suomalainen, C. J. Jorgez, M. M. Matzuk, S. Werner, I. Thesleff, Follistatin Regulates Enamel Patterning in Mouse Incisors by Asymmetrically Inhibiting BMP Signaling and Ameloblast Differentiation. *Dev. Cell* **7**, 719-730 (2004).
69. A. Hosoya, J.-Y. Kim, S.-W. Cho, H.-S. Jung, BMP4 signaling regulates formation of Hertwig's epithelial root sheath during tooth root development. *Cell Tissue Res.* **333**, 503-509 (2008).
70. Y. Chen, Y. Zhang, T.-X. Jiang, A. J. Barlow, T. R. St. Amand, Y. Hu, S. Heaney, P. Francis-West, C.-M. Chuong, R. Maas, Conservation of early odontogenic signaling pathways in Aves. *Proc. Natl. Acad. Sci. U. S. A.* **97**, 10044-10049 (2000).
71. W. R. Jackman, B. W. Draper, D. W. Stock, Fgf signaling is required for zebrafish tooth development. *Dev. Biol.* **274**, 139-157 (2004).
72. D. W. Stock, W. R. Jackman, J. Trapani, Developmental genetic mechanisms of evolutionary tooth loss in cypriniform fishes. *Development* **133**, 3127-3137 (2006).
73. Y. Li, X. Lü, X. Sun, S. Bai, S. Li, J. Shi, Odontoblast-like cell differentiation and dentin formation induced with TGF-β1. *Arch. Oral Biol.* **56**, 1221-1229 (2011).
74. S. G. Dobie K, Sloan AJ, Smith AJ, Effects of aliginate hydrogels and TGF-beta 1 on human dental pulp repair in vitro. *Connect Tissue Research* **43**, 387-390 (2002).
75. F. J. Unda, A. Martín, C. Hernandez, G. Pérez-Nanclares, E. Hilario, J. Aréchaga, FGFs-1 and -2, and TGFβ 1 as Inductive Signals Modulating in vitro Odontoblast Differentiation. *Adv. Dental Res.* **15**, 34-38 (2001).
76. H. He, J. Yu, Y. Liu, S. Lu, H. Liu, J. Shi, Y. Jin, Effects of FGF2 and TGFβ1 on the differentiation of human dental pulp stem cells in vitro. *Cell Biol. Int.* **32**, 827-834 (2008).
77. J. Štembírek, M. Kyllar, I. Putnová, L. Stehlík, M. Buchtová, The pig as an experimental model for clinical craniofacial research. *Lab. Anim.* **46**, 269-279 (2012).
78. J. Štembírek, M. Buchtová, T. Král, E. Matalová, S. Lozanoff, I. Míšek, Early morphogenesis of heterodont dentition in minipigs. *Eur. J. Oral Sci.* **118**, 547-558 (2010).

79. A. Nait Lechguer, S. Kuchler-Bopp, B. Hu, Y. Haïkel, H. Lesot, Vascularization of Engineered Teeth. *J. Dent. Res.* **87**, 1138-1143 (2008).
80. K. Nakao, R. Morita, Y. Saji, K. Ishida, Y. Tomita, M. Ogawa, M. Saitoh, Y. Tomooka, T. Tsuji, The development of a bioengineered organ germ method. *Nat Meth* **4**, 227-230 (2007).
81. E. Ikeda, R. Morita, K. Nakao, K. Ishida, T. Nakamura, T. Takano-Yamamoto, M. Ogawa, M. Mizuno, S. Kasugai, T. Tsuji, Fully functional bioengineered tooth replacement as an organ replacement therapy. *Proceedings of the National Academy of Sciences* **106**, 13475-13480 (2009).
82. M. Oshima, K. Inoue, K. Nakajima, T. Tachikawa, H. Yamazaki, T. Isobe, A. Sugawara, M. Ogawa, C. Tanaka, M. Saito, S. Kasugai, T. Takano-Yamamoto, T. Inoue, K. Tezuka, T. Kuboki, A. Yamaguchi, T. Tsuji, Functional tooth restoration by next-generation bio-hybrid implant as a bio-hybrid artificial organ replacement therapy. *Sci. Rep.* **4**, 6044 (2014).
83. T. Vos, A. D. Flaxman, M. Naghavi, R. Lozano, C. Michaud, M. Ezzati, K. Shibuya, J. A. Salomon, S. Abdalla, V. Aboyans, J. Abraham, I. Ackerman, R. Aggarwal, S. Y. Ahn, M. K. Ali, M. A. AlMazroa, M. Alvarado, H. R. Anderson, L. M. Anderson, K. G. Andrews, C. Atkinson, L. M. Baddour, A. N. Bahalim, S. Barker-Collo, L. H. Barrero, D. H. Bartels, M.-G. Basáñez, A. Baxter, M. L. Bell, E. J. Benjamin, D. Bennett, E. Bernabé, K. Bhalla, B. Bhandari, B. Bikbov, A. B. Abdulhak, G. Birbeck, J. A. Black, H. Blencowe, J. D. Blore, F. Blyth, I. Bolliger, A. Bonaventure, S. Boufous, R. Bourne, M. Boussinesq, T. Braithwaite, C. Brayne, L. Bridgett, S. Brooker, P. Brooks, T. S. Brugha, C. Bryan-Hancock, C. Bucello, R. Buchbinder, G. Buckle, C. M. Budke, M. Burch, P. Burney, R. Burstein, B. Calabria, B. Campbell, C. E. Canter, H. Carabin, J. Carapetis, L. Carmona, C. Cella, F. Charlson, H. Chen, A. T.-A. Cheng, D. Chou, S. S. Chugh, L. E. Coffeng, S. D. Colan, S. Colquhoun, K. E. Colson, J. Condon, M. D. Connor, L. T. Cooper, M. Corriere, M. Cortinovis, K. C. de Vaccaro, W. Couser, B. C. Cowie, M. H. Criqui, M. Cross, K. C. Dabhadkar, M. Dahiya, N. Dahodwala, J. Damsere-Derry, G. Danaei, A. Davis, D. De Leo, L. Degenhardt, R. Dellavalle, A. Delossantos, J. Denenberg, S. Derrett, D. C. Des Jarlais, S. D. Dharmaratne, M. Dherani, C. Diaz-Torne, H. Dolk, E. R. Dorsey, T. Driscoll, H. Duber, B. Ebel, K. Edmond, A. Elbaz, S. E. Ali, H. Erskine, P. J. Erwin, P. Espindola, S. E. Ewoigbokhan, F. Farzadfar, V. Feigin, D. T. Felson, A. Ferrari, C. P. Ferri, E. M. Fèvre, M. M. Finucane, S. Flaxman, L. Flood, K. Foreman, M. H. Forouzanfar, F. G. R. Fowkes, R. Franklin, M. Fransen, M. K. Freeman, B. J. Gabbe, S. E. Gabriel, E. Gakidou, H. A. Ganatra, B. Garcia, F. Gaspari, R. F. Gillum, G. Gmel, R. Gosselin, R. Grainger, J. Groeger, F. Guillemin, D. Gunnell, R. Gupta, J. Haagsma, H. Hagan, Y. A. Halasa, W. Hall, D. Haring, J. M. Haro, J. E. Harrison, R. Havmoeller, R. J. Hay, H. Higashi, C. Hill, B. Hoen, H. Hoffman, P. J. Hotez, D. Hoy, J. J. Huang, S. E. Ibeanusi, K. H. Jacobsen, S. L. James, D. Jarvis, R. Jasrasaria, S. Jayaraman, N. Johns, J. B. Jonas, G. Karthikeyan, N. Kassebaum, N. Kawakami, A. Keren, J.-P. Khoo, C. H. King, L. M. Knowlton, O. Kobusingye, A. Koranteng, R. Krishnamurthi, R. Lalloo, L. L. Laslett, T.

Lathlean, J. L. Leasher, Y. Y. Lee, J. Leigh, S. S. Lim, E. Limb, J. K. Lin, M. Lipnick, S. E. Lipshultz, W. Liu, M. Loane, S. L. Ohno, R. Lyons, J. Ma, J. Mabweijano, M. F. MacIntyre, R. Malekzadeh, L. Mallinger, S. Manivannan, W. Marcenes, L. March, D. J. Margolis, G. B. Marks, R. Marks, A. Matsumori, R. Matzopoulos, B. M. Mayosi, J. H. McAnulty, M. M. McDermott, N. McGill, J. McGrath, M. E. Medina-Mora, M. Meltzer, Z. A. Memish, G. A. Mensah, T. R. Merriman, A.-C. Meyer, V. Miglioli, M. Miller, T. R. Miller, P. B. Mitchell, A. O. Mocumbi, T. E. Moffitt, A. A. Mokdad, L. Monasta, M. Montico, M. Moradi-Lakeh, A. Moran, L. Morawska, R. Mori, M. E. Murdoch, M. K. Mwaniki, K. Naidoo, M. N. Nair, L. Naldi, K. M. V. Narayan, P. K. Nelson, R. G. Nelson, M. C. Nevitt, C. R. Newton, S. Nolte, P. Norman, R. Norman, M. O'Donnell, S. O'Hanlon, C. Olives, S. B. Omer, K. Ortblad, R. Osborne, D. Ozgediz, A. Page, B. Pahari, J. D. Pandian, A. P. Rivero, S. B. Patten, N. Pearce, R. P. Padilla, F. Perez-Ruiz, N. Perico, K. Pesudovs, D. Phillips, M. R. Phillips, K. Pierce, S. Pion, G. V. Polanczyk, S. Polinder, C. A. Pope Iii, S. Popova, E. Porrini, F. Pourmalek, M. Prince, R. L. Pullan, K. D. Ramaiah, D. Ranganathan, H. Razavi, M. Regan, J. T. Rehm, D. B. Rein, G. Remuzzi, K. Richardson, F. P. Rivara, T. Roberts, C. Robinson, F. R. De Leòn, L. Ronfani, R. Room, L. C. Rosenfeld, L. Rushton, R. L. Sacco, S. Saha, U. Sampson, L. Sanchez-Riera, E. Sanman, D. C. Schwebel, J. G. Scott, M. Segui-Gomez, S. Shahraz, D. S. Shepard, H. Shin, R. Shivakoti, D. Silberberg, D. Singh, G. M. Singh, J. A. Singh, J. Singleton, D. A. Sleet, K. Sliwa, E. Smith, J. L. Smith, N. J. C. Stapelberg, A. Steer, T. Steiner, W. A. Stolk, L. J. Stovner, C. Sudfeld, S. Syed, G. Tamburlini, M. Tavakkoli, H. R. Taylor, J. A. Taylor, W. J. Taylor, B. Thomas, W. M. Thomson, G. D. Thurston, I. M. Tleyjeh, M. Tonelli, J. A. Towbin, T. Truelsen, M. K. Tsilimbaris, C. Ubeda, E. A. Undurraga, M. J. van der Werf, J. van Os, M. S. Vavilala, N. Venketasubramanian, M. Wang, W. Wang, K. Watt, D. J. Weatherall, M. A. Weinstock, R. Weintraub, M. G. Weisskopf, M. M. Weissman, R. A. White, H. Whiteford, S. T. Wiersma, J. D. Wilkinson, H. C. Williams, S. R. M. Williams, E. Witt, F. Wolfe, A. D. Woolf, S. Wulf, P.-H. Yeh, A. K. M. Zaidi, Z.-J. Zheng, D. Zonies, A. D. Lopez, C. J. L. Murray, Years lived with disability (YLDs) for 1160 sequelae of 289 diseases and injuries 1990–2010: a systematic analysis for the Global Burden of Disease Study 2010. *The Lancet* **380**, 2163-2196 (2012).

84. P. E. Murray, F. Garcia-Godoy, K. M. Hargreaves, Regenerative Endodontics: A Review of Current Status and a Call for Action. *Journal of Endodontics* **33**, 377-390 (2007).

85. J. W. Nichol, S. T. Koshy, H. Bae, C. M. Hwang, S. Yamanlar, A. Khademhosseini, Cell-laden microengineered gelatin methacrylate hydrogels. *Biomaterials* **31**, 5536-5544 (2010).

86. V. Hosseini, S. Ahadian, S. Ostrovidov, G. Camci-Unal, S. Chen, H. Kaji, M. Ramalingam, A. Khademhosseini, Engineered Contractile Skeletal Muscle Tissue on a Microgrooved Methacrylated Gelatin Substrate. *Tissue Engineering Part A* **18**, 2453-2465 (2012).

87. S. R. Shin, S. M. Jung, M. Zalabany, K. Kim, P. Zorlutuna, S. b. Kim, M. Nikkhah, M. Khabiry, M. Azize, J. Kong, K.-t. Wan, T. Palacios, M. R. Dokmeci, H. Bae, X. Tang, A. Khademhosseini, Carbon-Nanotube-Embedded Hydrogel Sheets for Engineering Cardiac Constructs and Bioactuators. *ACS Nano* **7**, 2369-2380 (2013).
88. J. Visser, D. Gawlitta, K. E. M. Benders, S. M. H. Toma, B. Pouran, P. R. van Weeren, W. J. A. Dhert, J. Malda, Endochondral bone formation in gelatin methacrylamide hydrogel with embedded cartilage-derived matrix particles. *Biomaterials* **37**, 174-182 (2015).
89. Y.-C. Chen, R.-Z. Lin, H. Qi, Y. Yang, H. Bae, J. M. Melero-Martin, A. Khademhosseini, Functional Human Vascular Network Generated in Photocrosslinkable Gelatin Methacrylate Hydrogels. *Advanced Functional Materials* **22**, 2027-2039 (2012).
90. D. Nguyen, Y. M. Akay, M. Akay, Investigating Glioblastoma Angiogenesis Using A 3D in Vitro Gelma Microwell Platform. *IEEE Trans. NanoBiosci.* **PP**, 1-1 (2016).
91. E. Manzke, E. Katchburian, F. P. Faria, E. Freymüller, Structural features of forming and developing blood capillaries of the enamel organ of rat molar tooth germs observed by light and electron microscopy. *J. Morphol.* **265**, 335-342 (2005).
92. S. Yoshida, H. Ohshima, S. Kobayashi, Vascularization of the Enamel Organ in Developing Molar Teeth of Rats -Scanning Electron Microscope Study of Corrosion Casts. *Okajimas Folia Anat. Jpn.* **66**, 99-111 (1989).
93. J. D. Decker, The development of a vascular supply to the rat molar enamel organ: An electron microscopic study. *Arch. Oral Biol.* **12**, 453-IN412 (1967).
94. X. Zhang, J. Yang, Y. Li, S. Liu, K. Long, Q. Zhao, Y. Zhang, Z. Deng, Y. Jin, Functional Neovascularization in Tissue Engineering with Porcine Acellular Dermal Matrix and Human Umbilical Vein Endothelial Cells. *Tissue Eng Part C Methods* **17**, 423-433 (2010).
95. J. Rouwkema, J. De Boer, C. A. Van Blitterswijk, Endothelial Cells Assemble into a 3-Dimensional Prevascular Network in a Bone Tissue ENgineering Construct. *Tissue Eng.* **12**, 2685-2693 (2006).
96. J. E. Marturano, J. D. Arena, Z. A. Schiller, I. Georgakoudi, C. K. Kuo, Characterization of mechanical and biochemical properties of developing embryonic tendon. *Proceedings of the National Academy of Sciences* **110**, 6370-6375 (2013).
97. W. C. Oliver, G. M. Pharr, An improved technique for determining hardness and elastic modulus using load and displacement sensing indentation experiments. *Journal of Materials Research* **7**, 1564-1583 (1992).
98. W. Zhang, I. P. Ahluwalia, P. C. Yelick, Three dimensional dental epithelial-mesenchymal constructs of predetermined size and shape for tooth regeneration. *Biomaterials* **31**, 7995-8003 (2010).
99. E. E. Smith, P. C. Yelick, A. Khademhosseini, in *Bioengineering Conference (NEBEC), 2014 40th Annual Northeast*. (2014), pp. 1-2.

100. M. Ahearne, Introduction to cell–hydrogel mechanosensing. *Interface Focus* **4**, 20130038 (2014).
101. M. Ahearne, K.-K. Liu, A. J. El Haj, K. Y. Then, S. Rauz, Y. Yang, Online Monitoring of the Mechanical Behavior of Collagen Hydrogels: Influence of Corneal Fibroblasts on Elastic Modulus. *Tissue Engineering Part C: Methods* **16**, 319-327 (2009).
102. C. Chung, E. Anderson, R. R. Pera, B. L. Pruitt, S. C. Heilshorn, Hydrogel crosslinking density regulates temporal contractility of human embryonic stem cell-derived cardiomyocytes in 3D cultures. *Soft matter* **8**, 10141-10148 (2012).
103. R. V. Ulijn, N. Bibi, V. Jayawarna, P. D. Thornton, S. J. Todd, R. J. Mart, A. M. Smith, J. E. Gough, Bioresponsive hydrogels. *Materials Today* **10**, 40-48 (2007).
104. L. E. Randall, R. C. Hall, Temperospatial Expression of Matrix Metalloproteinases 1, 2, 3, and 9 During Early Tooth Development. *Connect. Tissue Res.* **43**, 205-211 (2002).
105. N. Yoshiba, K. Yoshiba, C. Stoetzel, F. Perrin-Schmitt, Y. Cam, J. V. Ruch, H. Lesot, Temporospatial gene expression and protein localization of matrix metalloproteinases and their inhibitors during mouse molar tooth development. *Dev. Dyn.* **228**, 105-112 (2003).
106. J. D. Bartlett, J. P. Simmer, Proteinases in Developing Dental Enamel. *Crit. Rev. Oral Biol. Medicine* **10**, 425-441 (1999).
107. M. Lovett, K. Lee, A. Edwards, D. L. Kaplan, Vascularization Strategies for Tissue Engineering. *Tissue Engineering. Part B, Reviews* **15**, 353-370 (2009).
108. E. C. Novosel, C. Kleinhans, P. J. Kluger, Vascularization is the key challenge in tissue engineering. *Adv. Drug Del. Rev.* **63**, 300-311 (2011).
109. J. M. Melero-Martin, M. E. De Obaldia, S.-Y. Kang, Z. A. Khan, L. Yuan, P. Oettgen, J. Bischoff, Engineering robust and functional vascular networks in vivo with human adult and cord blood-derived progenitor cells. *Circul. Res.* **103**, 194-202 (2008).
110. C. Hahn, M. A. Schwartz, Mechanotransduction in vascular physiology and atherogenesis. *Nature reviews. Molecular cell biology* **10**, 53-62 (2009).
111. G. R. Drummond, S. Selemidis, K. K. Griendling, C. G. Sobey, Combating oxidative stress in vascular disease: NADPH oxidases as therapeutic targets. *Nature Reviews. Drug Discovery* **10**, 453-471 (2011).
112. R.-Z. Lin, Y.-C. Chen, R. Moreno-Luna, A. Khademhosseini, J. M. Melero-Martin, Transdermal regulation of vascular network bioengineering using a photopolymerizable methacrylated gelatin hydrogel. *Biomaterials* **34**, 6785-6796 (2013).
113. S. Levenberg, J. Rouwkema, M. Macdonald, E. S. Garfein, D. S. Kohane, D. C. Darland, R. Marini, C. A. van Blitterswijk, R. C. Mulligan, P. A. D'Amore, R. Langer, Engineering vascularized skeletal muscle tissue. *Nat Biotech* **23**, 879-884 (2005).
114. S. Dimitrova-Nakov, A. Baudry, Y. Harichane, O. Kellermann, M. Goldberg, Pulp Stem Cells: Implication in Reparative Dentin Formation. *Journal of Endodontics* **40**, S13-S18 (2014).

115. J. Yu, Y. Wang, Z. Deng, L. Tang, Y. Li, J. Shi, Y. Jin, Odontogenic capability: bone marrow stromal stem cells versus dental pulp stem cells. *Biol. Cell* **99**, 465-474 (2007).
116. B. Trappmann, C. S. Chen, How cells sense extracellular matrix stiffness: a material's perspective. *Curr. Opin. Biotechnol.* **24**, 948-953 (2013).
117. L. B. Hazeltine, J. A. Selekman, S. P. Palecek, Engineering the human pluripotent stem cell microenvironment to direct cell fate. *Biotechnol. Adv.* **31**, 1002-1019 (2013).
118. R. G. Wells, The role of matrix stiffness in regulating cell behavior. *Hepatology* **47**, 1394-1400 (2008).
119. M. P. Lutolf, J. A. Hubbell, Synthetic biomaterials as instructive extracellular microenvironments for morphogenesis in tissue engineering. *Nat Biotech* **23**, 47-55 (2005).
120. F. Brandl, F. Sommer, A. Goepferich, Rational design of hydrogels for tissue engineering: Impact of physical factors on cell behavior. *Biomaterials* **28**, 134-146 (2007).
121. Y. Sun, C. S. Chen, J. Fu, Forcing Stem Cells to Behave: A Biophysical Perspective of the Cellular Microenvironment. *Annual Review of Biophysics* **41**, 519-542 (2012).
122. B. R. Chrcanovic, T. Albrektsson, A. Wennerberg, Reasons for failures of oral implants. *J. Oral Rehabil.* **41**, 443-476 (2014).
123. M. Esposito, H. Maghaireh, M. G. Grusovin, I. Ziounas, H. V. Worthington, Interventions for replacing missing teeth: management of soft tissues for dental implants. *Cochrane Database of Systematic Reviews*, (2012).
124. B. R. Chrcanovic, J. Kisch, T. Albrektsson, A. Wennerberg, Factors Influencing Early Dental Implant Failures. *J. Dent. Res.* **95**, 995-1002 (2016).
125. E. E. Smith, P. C. Yelick, Progress in Bioengineered Whole Tooth Research: from Bench to Dental Patient Chair. *Current Oral Health Reports*, 1-7 (2016).
126. E. E. Smith, W. Zhang, N. R. Schiele, A. Khademhosseini, C. K. Kuo, P. C. Yelick, Developing a biomimetic tooth bud model. *Journal of Tissue Engineering and Regenerative Medicine*, n/a-n/a (2017).
127. F. Luo, T.-Y. Hou, Z.-H. Zhang, Z. Xie, X.-H. Wu, J.-Z. Xu, Effects of Initial Cell Density and Hydrodynamic Culture on Osteogenic Activity of Tissue-Engineered Bone Grafts. *PLoS One* **8**, e53697 (2013).
128. M. A. Yassin, K. N. Leknes, T. O. Pedersen, Z. Xing, Y. Sun, S. A. Lie, A. Finne-Wistrand, K. Mustafa, Cell seeding density is a critical determinant for copolymer scaffolds-induced bone regeneration. *Journal of Biomedical Materials Research Part A* **103**, 3649-3658 (2015).
129. S. Talukdar, Q. T. Nguyen, A. C. Chen, R. L. Sah, S. C. Kundu, Effect of initial cell seeding density on 3D-engineered silk fibroin scaffolds for articular cartilage tissue engineering. *Biomaterials* **32**, 8927-8937 (2011).
130. M. J. Harding, H. F. McGraw, A. Nechiporuk, The roles and regulation of multicellular rosette structures during morphogenesis. *Development* **141**, 2549 (2014).

131. Y. Chen, Z. Wang, Y. Xie, X. Guo, X. Tang, S. Wang, S. Yang, K. Chen, Y. Niu, W. Ji, Folic acid deficiency inhibits neural rosette formation and neuronal differentiation from rhesus monkey embryonic stem cells. *J. Neurosci. Res.* **90**, 1382-1391 (2012).
132. J. T. Blankenship, S. T. Backovic, Justina S. P. Sanny, O. Weitz, J. A. Zallen, Multicellular Rosette Formation Links Planar Cell Polarity to Tissue Morphogenesis. *Dev. Cell* **11**, 459-470 (2006).
133. J. Prochazka, M. Prochazkova, W. Du, F. Spoutil, J. Tureckova, R. Hoch, T. Shimogori, R. Sedlacek, John L. Rubenstein, T. Wittmann, Ophir D. Klein, Migration of Founder Epithelial Cells Drives Proper Molar Tooth Positioning and Morphogenesis. *Dev. Cell* **35**, 713-724 (2015).
134. M. G. Chavez, W. Yu, B. Biehs, H. Harada, M. L. Snead, J. S. Lee, T. A. Desai, O. D. Klein, Characterization of Dental Epithelial Stem Cells from the Mouse Incisor with Two-Dimensional and Three-Dimensional Platforms. *Tissue Engineering Part C: Methods* **19**, 15-24 (2012).
135. E. Juuri, K. Saito, L. Ahtiainen, K. Seidel, M. Tummers, K. Hochedlinger, O. D. Klein, I. Thesleff, F. Michon, Sox2+ Stem Cells Contribute to All Epithelial Lineages of the Tooth via Sfrp5+ Progenitors. *Dev. Cell* **23**, 317-328 (2012).
136. E. Seo, U. Basu-Roy, J. Zavadil, C. Basilico, A. Mansukhani, Distinct Functions of Sox2 Control Self-Renewal and Differentiation in the Osteoblast Lineage. *Mol. Cell. Biol.* **31**, 4593-4608 (2011).
137. Z. Sun, W. Yu, M. Sanz Navarro, M. Sweat, S. Eliason, T. Sharp, H. Liu, K. Seidel, L. Zhang, M. Moreno, T. Lynch, N. E. Holton, L. Rogers, T. Neff, M. J. Goodheart, F. Michon, O. D. Klein, Y. Chai, A. Dupuy, J. F. Engelhardt, Z. Chen, B. A. Amendt, Sox2 and Lef-1 interact with Pitx2 to regulate incisor development and stem cell renewal. *Development* **143**, 4115 (2016).
138. E. Juuri, M. Jussila, K. Seidel, S. Holmes, P. Wu, J. Richman, K. Heikinheimo, C.-M. Chuong, K. Arnold, K. Hochedlinger, O. Klein, F. Michon, I. Thesleff, Sox2 marks epithelial competence to generate teeth in mammals and reptiles. *Development* **140**, 1424 (2013).
139. C. Huang, D. Qin, Role of Lef1 in sustaining self-renewal in mouse embryonic stem cells. *Journal of Genetics and Genomics* **37**, 441-449 (2010).
140. T. Sasaki, Y. Ito, X. Xu, J. Han, P. Bringas Jr, T. Maeda, H. C. Slavkin, R. Grosschedl, Y. Chai, LEF1 is a critical epithelial survival factor during tooth morphogenesis. *Dev. Biol.* **278**, 130-143 (2005).
141. X.-P. Wang, M. Suomalainen, S. Felszeghy, L. C. Zelarayan, M. T. Alonso, M. V. Plikus, R. L. Maas, C.-M. Chuong, T. Schimmang, I. Thesleff, An Integrated Gene Regulatory Network Controls Stem Cell Proliferation in Teeth. *PLoS Biol.* **5**, e159 (2007).
142. P. Kettunen, J. Laurikkala, P. Itäranta, S. Vainio, N. Itoh, I. Thesleff, Associations of FGF-3 and FGF-10 with signaling networks regulating tooth morphogenesis. *Dev. Dyn.* **219**, 322-332 (2000).

143. C.-Y. Li, W. Cha, H.-U. Luder, R.-P. Charles, M. McMahon, T. A. Mitsiadis, O. D. Klein, E-cadherin regulates the behavior and fate of epithelial stem cells and their progeny in the mouse incisor. *Dev. Biol.* **366**, 357-366 (2012).
144. L. Ahtiainen, I. Uski, I. Thesleff, M. L. Mikkola, Early epithelial signaling center governs tooth budding morphogenesis. *The Journal of Cell Biology* **214**, 753 (2016).
145. J. Y. F. Chang, C. Wang, J. Liu, Y. Huang, C. Jin, C. Yang, B. Hai, F. Liu, R. N. D'Souza, W. L. McKeehan, F. Wang, Fibroblast Growth Factor Signaling Is Essential for Self-renewal of Dental Epithelial Stem Cells. *The Journal of Biological Chemistry* **288**, 28952-28961 (2013).
146. K. Kratochwil, J. Galceran, S. Tontsch, W. Roth, R. Grosschedl, FGF4, a direct target of LEF1 and Wnt signaling, can rescue the arrest of tooth organogenesis in Lef1(−/−) mice. *Genes Dev.* **16**, 3173-3185 (2002).
147. T. Åberg, X.-P. Wang, J.-H. Kim, T. Yamashiro, M. Bei, R. Rice, H.-M. Ryoo, I. Thesleff, Runx2 mediates FGF signaling from epithelium to mesenchyme during tooth morphogenesis. *Dev. Biol.* **270**, 76-93 (2004).
148. M. Tamura, E. Nemoto, Role of the Wnt signaling molecules in the tooth. *The Japanese Dental Science Review* **52**, 75-83 (2016).
149. B. Namkoong, S. Güven, S. Ramesan, V. Liaudanskaya, A. Abzhanov, U. Demirci, Recapitulating cranial osteogenesis with neural crest cells in 3-D microenvironments. *Acta Biomater.* **31**, 301-311 (2016).
150. K. Kim, D. Dean, A. G. Mikos, J. P. Fisher, Effect of Initial Cell Seeding Density on Early Osteogenic Signal Expression of Rat Bone Marrow Stromal Cells Cultured on Cross-Linked Poly(propylene fumarate) Disks. *Biomacromolecules* **10**, 1810-1817 (2009).
151. J. Rouwkema, J. D. Boer, C. A. V. Blitterswijk, Endothelial Cells Assemble into a 3-Dimensional Prevascular Network in a Bone Tissue Engineering Construct. *Tissue Eng.* **12**, 2685-2693 (2006).
152. M. Petersson, H. Brylka, A. Kraus, S. John, G. Rappl, P. Schettina, C. Niemann, TCF/Lef1 activity controls establishment of diverse stem and progenitor cell compartments in mouse epidermis. *The EMBO Journal* **30**, 3004-3018 (2011).
153. M. Kira-Tatsuoka, K. Oka, E. Tsuruga, M. Ozaki, Y. Sawa, Immunohistochemical expression of fibrillin-1 and fibrillin-2 during tooth development. *Journal of Periodontal Research* **50**, 714-720 (2015).
154. J. Li, J. Feng, Y. Liu, T.-V. Ho, W. Grimes, Hoang A. Ho, S. Park, S. Wang, Y. Chai, BMP-SHH Signaling Network Controls Epithelial Stem Cell Fate via Regulation of Its Niche in the Developing Tooth. *Dev. Cell* **33**, 125-135.
155. H. Harada, P. Kettunen, H.-S. Jung, T. Mustonen, Y. A. Wang, I. Thesleff, Localization of Putative Stem Cells in Dental Epithelium and Their Association with Notch and Fgf Signaling. *The Journal of Cell Biology* **147**, 105-120 (1999).